J Solid State Electrochem (2000) 4: 243–266

REVIEW

Vladislav V. Kharton · Aleksey A. Yaremchenko
Evgeny N. Naumovich · Fernando M. B. Marques

Research on the electrochemistry of oxygen ion conductors in the former Soviet Union

III. HfO_2-, CeO_2- and ThO_2-based oxides

Received: 23 September 1999 / Accepted: 10 October 1999

Abstract This review is focused on the analysis of experimental results on oxygen ion-conducting ceramic materials based on HfO_2, CeO_2, and ThO_2, published in the former Soviet Union. In particular, the physicochemical and transport properties of fluorite-related oxides and the characteristics of electronic conduction in these solid electrolytes are briefly reviewed. Emphasis is given to electrocatalytic and electrochemical properties of cerium-containing oxides, which are promising materials for electrodes of electrochemical cells operating in reducing atmospheres, and mixed-conducting membranes. A comparative analysis of specific features of the solid-electrolyte ceramics based on hafnia, zirconia, ceria, and thoria is performed in order to reveal basic tendencies of oxygen ionic transport in fluorite-type oxides, and to identify the potential applicability of these materials in various high-temperature electrochemical devices.

Key words Stabilized hafnia · Doped ceria · Thoria · Solid electrolyte · Ionic conductivity

Introduction

Oxygen ion-conducting solid electrolytes find numerous technological applications in solid oxide fuel cells (SOFCs), sensors of various types, high-temperature electrolyzers, and ceramic membranes for partial oxidation of hydrocarbons. Each of these applications has specific requirements in terms of materials properties. In particular, the main requirement for solid electrolytes used in SOFCs and sensors is maximum oxygen ionic conductivity and minimum electronic conduction under typical operating conditions. On the other hand, the ability to optimize properties of ion-conducting materials is relatively limited, and both construction and performance of electrochemical cells are often determined by the properties of materials available. Therefore, the development of materials with satisfactory properties for high-temperature electrochemical applications is an important scientific task. At the same time, numerous results in this field obtained in the former Soviet Union, and published mainly in Russian, are practically unknown to Western scientists.

This work focused on studies on oxygen ion-conducting ceramic materials based on HfO_2, CeO_2, and ThO_2, performed in the former USSR. Among other goals, the authors tried to analyze the results considered of present interest for the state-of-the-art in the field of high-temperature electrochemistry of oxygen. Particular emphasis was also given to list briefly a number of articles published in less-known issues and journals, in order to assist people looking for information on these themes. In this review, no attempt was made to compare the results obtained in Soviet and Western scientific centers. Such comparison would obviously show enormous coherence between such results, as any reader familiar to the subject might conclude from the present paper. Lastly, references to papers published in international journals included in this work were only selected to show relationships between selected sets of experimental results.

V.V. Kharton[1] (✉) · A.A. Yaremchenko · E.N. Naumovich
Institute of Physicochemical Problems,
Belarus State University, 14 Leningradskaya Str.,
220080 Minsk, Republic of Belarus
e-mail: kharton@cv.ua.pt
Tel.: +351-34-370263; Fax: +351-34-425300

F.M.B. Marques
Department of Ceramics and Glass Engineering,
UIMC, University of Aveiro, 3810-193 Aveiro, Portugal

Present address:
[1] Department of Ceramics and Glass Engineering,
UIMC, University of Aveiro, 3810-193 Aveiro, Portugal

HfO_2-based ceramic materials

Most of the phase relationships in the oxide systems based on hafnium dioxide are close to those found in

Table 1 Oxygen ion transference numbers of HfO_2 in different atmospheres determined from the e.m.f. of oxygen concentration cells

Atmosphere	t_O							Ref.
	973 K	1023 K	1073 K	1123 K	1173 K	1223 K	1273 K	
O_2/air	0.31	0.26	0.23	0.16	0.14	0.11	0.09	[9]
O_2/air	0.12	–	0.10	0.07	0.06	0.04	0.03	[8]
O_2/CO + CO_2 (10% CO)	0.73	0.67	0.69	0.61	0.59	0.43	0.35	[8]
O_2/CO + CO_2 (66% CO)	0.82	–	0.75	–	0.60	–	0.49	[8]

zirconia-based oxides, discussed in the Part I of this review [1]; the properties of these groups of oxides are also alike, owing to the similar electronic configuration of zirconium and hafnium cations. However, HfO_2-based ceramics have found fewer electrochemical applications than zirconia owing to several important differences in the transport properties and stability of these materials. Firstly, the oxygen ionic conductivity of the most-conducting solid electrolytes of stabilized hafnia, with the fluorite-type structure, is significantly lower than that of zirconia-based oxides. Secondly, stabilized fluorite-type phases of hafnium dioxide, having the highest ionic conductivity, are less stable at low temperatures than those based on stabilized zirconia. Another significant difference is a considerably higher chemical stability and mechanical strength of HfO_2-based ceramics with respect to stabilized ZrO_2, which could enhance the applicability domain of these materials, but also prevents the easy synthesis and processing of hafnia-based ceramics.

When reviewing the literature on HfO_2-containing oxides, one should mention separately a monograph [2], which presents a large amount of data on phase diagrams, kinetics of solid-state synthesis and properties of these materials.

Hafnium dioxide and the systems HfO_2-MO (M = Be, Mg, Ca, Sr, Ba)

As found for zirconium dioxide, HfO_2 has a monoclinic structure at low temperature; increasing the temperature results in a transition of the monoclinic (M) phase to tetragonal (T) and then to a cubic fluorite-type (F) phase [2, 3]. However, the temperatures for $M \rightarrow T$ and $T \rightarrow F$ phase transitions for hafnia are higher than those for zirconia: the $M \rightarrow T$ transformation for HfO_2 takes place at approximately 2100–2270 K, depending on impurity content, and the cubic phase of HfO_2 forms only at temperatures close to the melting point ($\sim$2970 K). Under high pressure (40–110 kbar) and at temperatures up to 1970 K, an orthorhombic phase can be obtained [4]. This phase, being metastable at ordinary conditions, decomposes rapidly when heating, even at temperatures as low as 770 K. Thermodynamic properties of hafnium dioxide and other oxides of the binary Hf-O system have been reported [5–7].

In oxidizing conditions, monoclinic HfO_2 shows mixed oxygen ionic and p-type electronic conductivity; the oxygen ion transference numbers in air do not exceed 0.3 at 970–1270 K (Table 1). The total electrical conductivity of monoclinic HfO_2 decreases with reducing oxygen partial pressure owing to decreasing p-type conductivity, which can be approximated by [8]:

$$\sigma_p = 35.5 p_{O_2}^{1/4} \exp\left(-\frac{15780}{T}\right) \quad (1)$$

with the pre-exponential term expressed in S cm^{-1} atm$^{-1/4}$. The activation energy for hole conduction in undoped hafnia is higher than for ionic transport [8]. As a result, the ion transference number of HfO_2 increases with decreasing oxygen pressure and temperature. Thermal expansion coefficients (TECs) of hafnium dioxide, determined from dilatometric [10] and high-temperature X-ray diffraction [11, 12] data, are given in Table 2.

The HfO_2 F-phase, which is the most interesting as a solid electrolyte in the hafnia-based oxide systems, can be stabilized to temperatures lower than the pure hafnium dioxide T↔F transition temperature, by addition of rare-earth or some alkaline-earth metal oxides.

Phase diagrams and selected phase relationships in the binary systems HfO_2-MO (M = Be, Mg, Ca, Sr, Ba) have been reported [13, 15, 16, 18–39]. Numerous research articles presented detailed ternary phase diagrams like HfO_2-ZrO_2-MgO [16], HfO_2-ZrO_2-CaO [18], HfO_2-Y_2O_3-MgO [35, 36], HfO_2-Y_2O_3-CaO [25, 26, 31–34, 38], or separate phase relationships in these systems. Thermodynamic properties of different hafnia-based oxide phases, stability, and kinetics of solid-state reactions involved in their synthesis were studied under various conditions [13, 23, 40–51]. When summarizing these results and comparing them to data on zirconia-based ceramics [1], one can select the following specific features:

1. In the phase diagrams with hafnia, the domains of formation of tetragonal and cubic fluorite-type solid solutions are shifted to higher temperatures in comparison to those of zirconia (Fig. 1). For a given temperature, the concentration range of the HfO_2-based fluorite phase is, as a rule, narrower than for the corresponding zirconia phase, and the minimum dopant concentration necessary to stabilize the F-phase is higher for hafnia. This results in poor stability of the hafnia-based fluorites at temperatures below 1600 K, in comparison with the corresponding zirconia phases.
2. In the systems HfO_2-MO, there are no stable fluorite-type phases to be used as solid electrolytes in the

Table 2 Thermal expansion coefficients of HfO_2-based oxides[a]

Composition	Method	Average TEC values				Ref.
		T (K)	$\bar{\alpha} \times 10^6$ (K^{-1})			
HfO_2	D	293–1073	4.31			[9]
$SrHfO_3$	D	298–1473	9.9			[12]
$SrHf_{0.52}Zr_{0.48}O_3$	D	298–1473	9.95			[12]
$La_2Hf_2O_7$	D	293–1173	7.85			[13]
$Pr_2Hf_2O_7$	D	293–1173	9.13			[13]
$Nd_2Hf_2O_7$	D	293–1173	9.27			[13]
$Sm_2Hf_2O_7$	D	293–1173	10.60			[13]
$Eu_2Hf_2O_7$	D	293–1173	10.82			[13]
$Tb_2Hf_2O_7$	D	293–1173	8.50			[13]
$Dy_2Hf_2O_7$	D	293–1173	9.75			[13]
$Ho_2Hf_2O_7$	D	293–1173	9.75			[13]
$Er_2Hf_2O_7$	D	293–1173	9.65			[13]
$Yb_2Hf_2O_7$	D	293–1173	10.40			[13]
$Lu_2Hf_2O_7$	D	293–1173	11.80			[13]
$Y_2Hf_2O_7$	D	293–1173	8.72			[13]
			$\alpha_a \times 10^6$ (K^{-1})	$\alpha_b \times 10^6$ (K^{-1})	$\alpha_c \times 10^6$ (K^{-1})	
HfO_2	XRD	293–473/473–673	4.3/4.9	2.6/2.2	13.8/13.9	[11]
		673–873/873–1073	6.4/6.2	1.9/1.5	14.3/17.3	
		1073–1473	7.1	1.0	17.2	
HfO_2	XRD	300–1370	8.67	0.58	13.62	[10]
$Hf_{0.7}Zr_{0.3}O_2$	XRD	300–1370	8.39	0.29	12.26	[10]
$Hf_{0.90}Mg_{0.10}O_{1.90}$	XRD	293–1773	7.17	–	–	[15]
$Hf_{0.85}Mg_{0.15}O_{1.85}$	XRD	293–1773	6.95	–	–	[15]
$Hf_{0.80}Mg_{0.20}O_{1.80}$	XRD	293–1773	6.79	–	–	[15]
$Er_4Hf_3O_{12}$	XRD	293–1573	5.57	–	5.7	[16]
$Yb_4Hf_3O_{12}$	XRD	293–1573	5.91	–	5.98	[16]
$Lu_4Hf_3O_{12}$	XRD	293–1573	6.10	–	5.83	[16]
$Sc_4Hf_3O_{12}$	XRD	293–1573	4.58	–	5.48	[16]
$BaHfO_3$	XRD	293–1273	7.7	–	–	[14]
$BaHf_{0.8}Y_{0.2}O_{3-\delta}$	XRD	293–1273	8.3	–	–	[14]

[a] D is the dilatometric method; XRD is the high-temperature X-ray diffraction technique; α_a, α_b, and α_c are the TECs for the *a*-, *b*-, and *c*-axis of the crystal lattice, respectively

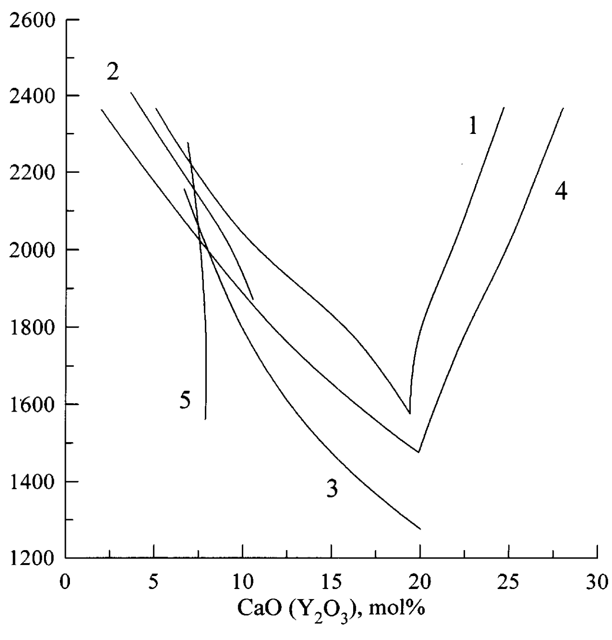

Fig. 1 Boundaries of the cubic fluorite phase formation domain: *1* HfO_2-CaO system [18]; *2* HfO_2-Y_2O_3 system [72]; *3* HfO_2-Y_2O_3 system [76]; *4* ZrO_2-CaO system [18]; *5* ZrO_2-Y_2O_3 system [150]

intermediate temperature range. For example, the fluorite solid solution $Hf_{0.81}Ca_{0.19}O_{1.81}$ is thermodynamically unstable at temperatures below 1630 K [43]. As found for the corresponding phase diagrams with zirconia, cubic fluorite-type solid solutions generally do not form in the systems with M = Be, Sr, Ba.

3. In contrast to the fluorite phases, the thermodynamic stability of perovskite-type hafnates $MHfO_3$ (M = Ca, Sr, Ba) is high with respect to the perovskite-like zirconates. Increasing ionic radius of alkaline-earth cations leads to increasing thermodynamic stability of the perovskite hafnates, as expected from geometrical constraints. Phase equilibria in the ternary oxide systems with hafnia and alkaline-earth metal oxides are determined by the perovskite phases having the highest thermodynamic stability in these systems.
4. Owing to thermodynamic reasons and the high kinetic stability of hafnium dioxide, the rate of formation of HfO_2-based fluorite solid-solutions is, as a rule, small with respect to the equivalent zirconia phases. Formation of the fluorite phases in the systems HfO_2-MO (M = Mg, Ca) occurs via intermediate perovskite phases.
5. As found for monoclinic zirconia, the solid solubility of alkaline-earth cations in the monoclinic hafnium

dioxide is very small. For instance, the concentration limit for magnesium and calcium cations in monoclinic HfO_2-based solid solutions does not exceed 1 mol% [16, 18].

Comparison of the transport properties of monoclinic hafnia ceramics containing different amounts of magnesia [8, 19, 52] shows that incorporation of magnesium cations leads to a clear but still small increase in the ionic conductivity. As a result, ion transference numbers of monoclinic HfO_2 increase with magnesia additions. The oxygen ionic conductivity of hafnia increases drastically when the monoclinic phase transforms to tetragonal [52]. The cubic solid solutions HfO_2-MgO, metastable at intermediate temperatures, exhibit predominant ionic conductivity, which is approximately independent of composition for magnesium concentrations higher than 15 mol% [19].

One should note that the segregation of beryllium and magnesium oxide phases in ceramics of HfO_2-MO (M = Be, Mg) systems, where no perovskite-type hafnates form, has little effect on the total conductivity of the ceramic materials [19]. At the same time, segregation of the perovskite phases in the ceramics of HfO_2-MO (M = Ca, Sr, Ba) results in a sharp decrease of the total conductivity [19], caused by the extremely high resistivity of the $MHfO_3$ perovskites. The perovskite-type hafnates exhibit mixed oxygen-ionic and p-type electronic conduction in air [15, 19, 25]. The values of the total conductivity of undoped hafnates are listed in Table 3.

Phase relationships in the HfO_2-Me_2O_3 (Me = La–Lu, Y, Sc) and HfO_2-ZrO_2 binary oxide systems, and related ternary systems

Phase diagrams, selected phase relationships, and the crystal structure of separate phases were reported for the systems HfO_2-Sc_2O_3 [17, 56–63], HfO_2-Y_2O_3 [56, 64–80], HfO_2-La_2O_3 [56, 75, 81–88], HfO_2-Ce_2O_3 (CeO_2) [89–92], HfO_2-PrO_x [56, 75, 81, 93–97], HfO_2-Nd_2O_3 [56, 75, 79, 81, 97–100], HfO_2-Sm_2O_3 [56, 75, 86, 96, 97, 101, 102], HfO_2-Eu_2O_3 [75, 103–105], HfO_2-Gd_2O_3 [56, 80, 86, 101, 106, 107], HfO_2-Tb_2O_3 [56, 79, 85, 101], HfO_2-Dy_2O_3 [56, 77, 79, 85, 86, 101, 120], HfO_2-Ho_2O_3 [64, 79, 85], HfO_2-Er_2O_3 [17, 56, 63, 64, 77, 79, 85, 86, 108, 109], HfO_2-Tm_2O_3 [62–64, 79, 85], HfO_2-Yb_2O_3 [17, 56, 62–64, 75, 77, 79, 80, 85, 110], HfO_2-Lu_2O_3 [17, 56, 62–64, 85, 96], HfO_2-ZrO_2 [111, 112], HfO_2-ZrO_2-Al_2O_3 [113, 114], HfO_2-ZrO_2-TiO_2 [115], HfO_2-ZrO_2-Sc_2O_3 [116], HfO_2-ZrO_2-Y_2O_3 [117, 118], HfO_2-Pr_2O_3-Dy_2O_3 [95], HfO_2-Y_2O_3-Al_2O_3 [74], and HfO_2-Y_2O_3-Ln_2O_3 (Ln = La, Er) [119, 121]. In the binary system HfO_2-ZrO_2 [111, 112] there are three continuous series of hafnia-zirconia solid solutions with monoclinic, tetragonal, and cubic fluorite structures. The continuous solid solubility is also typical for the isostructural zirconia- and hafnia-based phases in the ternary systems containing these components [113–118]. Here, the temperatures of the M $\rightarrow$ T and T $\rightarrow$ F phase transitions increase regularly with increasing hafnium concentration, being consistent with the properties of pure zirconia and hafnia phases.

Generally, the phase diagrams of hafnia with rare-earth element (REE) oxides are similar to the phase diagrams based on zirconium dioxide. Main features observed in the hafnia-rich parts of these diagrams may be summarized as follows:

1. All the phase diagrams are characterized by narrow fields of formation of solid solutions based on monoclinic and tetragonal HfO_2. The solid solubility of rare-earth oxides in these phases increases with increasing temperature and with increasing REE cation radius. For instance, the concentration range

Table 3 Total electrical conductivity of some HfO_2-based perovskites and pyrochlores

Composition	Total conductivity in air		Activation energy for the total electrical conductivity		Ref.
	T (K)	σ (S/cm)	T (K)	E_A (eV)	
$CaHfO_3$	1173	3.8×10^{-7}	773–1073	1.65	[19]
	1273	1.3×10^{-6}			
$SrHfO_3$	973	2.9×10^{-7}	773–923	1.55	[19]
	1173	7.4×10^{-6}	923–1273	1.1	
	1273	2.3×10^{-5}			
$BaHfO_3$	973	1.6×10^{-6}	773–1073	1.44	[19]
	1173	1.9×10^{-5}	1073–1273	1.0	
	1273	6.4×10^{-5}			
$La_2Hf_2O_7$	973	1.6×10^{-7}	970–1570	1.14	[53]
	973	4.4×10^{-7}	1173–1473	1.4	[83]
	1073	9.0×10^{-7}			
	1473	2.6×10^{-5}			
$Pr_2Hf_2O_7$	1073	5.4×10^{-5}	–	–	[54]
	1473	5.3×10^{-4}			
$Nd_2Hf_2O_7$	973	2.7×10^{-5}	773–973	1.07	[55]
	1073	8.2×10^{-5}	973–1273	0.87	
	973	4.4×10^{-6}	–	–	[98]
	1073	1.5×10^{-5}			
	1473	3.7×10^{-4}			

for La_2O_3 and Pr_2O_3 solid solutions in tetragonal hafnia corresponds to approximately 5–6 mol% at 1970–2270 K [81, 82, 94]. For other REE oxides, including neodimia, the maximum solid solubility in the tetragonal phase does not exceed 2 mol% [81, 101]. The solid solubility of REE cations in monoclinic hafnia is lower than for the tetragonal phase, as expected from geometrical characteristics of these structures. Addition of REE oxides leads to decreasing temperatures of the M $\rightarrow$ T and T $\rightarrow$ F phase transformations.

2. With respect to the zirconia-based phases, the temperatures of all phase transformations of the hafnia-based oxides are, as a rule, higher. As a result, full stabilization at intermediate temperatures of the F-phase in hafnia-containing systems requires larger additions of REE dopants (Fig. 1). Another consequence is that the most-conductive fluorite-type solid solutions, containing a minimum amount of stabilizing dopants, are less stable at low temperatures in the case of stabilized hafnia.
3. Several phases with the fluorite-derived structure, due to cation and/or anion ordering, form in the hafnia-rich side of the binary HfO_2-Me_2O_3 oxide systems. Among these phases, the most important are the pyrochlores, $Me_2Hf_2O_7$, and the so-called δ-phases, $Me_4Hf_3O_{12}$. As found for the zirconia-based systems, the stability of the hafnia-containing pyrochlores decreases with decreasing REE cation radius, whereas the behavior of the δ-phases is the opposite.
4. Formation of the $Me_2Hf_2O_7$ pyrochlore phases is observed for Me = La–Tb. In contrast to the fluorite-type phases, the pyrochlore hafnates ($Me_2Hf_2O_7$) are more stable than the zirconates ($Me_2Zr_2O_7$). In particular, an incongruent melting is characteristic for the samarium hafnate, $Sm_2Hf_2O_7$ [101, 122], whilst samarium zirconate shows an "order-disorder" phase transition, and transforms to fluorite at temperatures below the melting point [122]. Analogously, formation of the terbium hafnate is observed at temperatures below 2270 K [101], whereas the pyrochlore-type terbium zirconate does not form. In the system HfO_2-Y_2O_3 there is no pyrochlore phase, but the minimum conductivity, which is observed for the composition $2HfO_2$-Y_2O_3, typical of stoichiometric pyrochlore phases, suggests a partial cation ordering in this system [65, 76, 78, 122]. As found for the pyrochlore-type zirconates, all the HfO_2-based systems are characterized by relatively wide concentration ranges of solid solutions with the pyrochlore phases. These homogeneity ranges become narrower with increasing temperature and decreasing REE cation radius, when the stability of the pyrochlore phases decreases.
5. Formation of the $Me_4Hf_3O_{12}$ phases is observed for Me = Er, Tm, Yb, Lu, Sc [17, 58, 60–63, 122]. The hexagonal $Me_4Hf_3O_{12}$ (Me = Er-Lu) forms are due to partial cation ordering and total ordering of oxygen vacancies in the fluorite lattice. $Sc_4Hf_3O_{12}$ is characterized by a disordered cation sublattice and completely ordered oxygen sublattice [17]. Increasing temperature results in increasing disorder and, therefore, in the $\delta \rightarrow$ F phase transition. This transition temperature increases with decreasing radius of REE cations, reaching a maximum at $\sim$1940 K for $Sc_4Hf_3O_{12}$ [60]. The concentration range of solid solutions based on $Me_4Hf_3O_{12}$ compounds is negligible [17].

For REE-rich domains in HfO_2-Me_2O_3 (Me = Gd–Lu, Sc) phase diagrams, other types of cation ordering are observed, leading to formation of the $Me_5Hf_2O_{11.5}$ and Me_6HfO_{11} hexagonal phases [108, 122]. Upon heating, these phases transform to C-type rare-earth oxide solid solutions. For the HfO_2-Me_2O_3 systems rich in REE oxides, at temperatures above 2000–2050 K, only solid solutions based on various phase modifications of REE oxides were found [56].

As found for the ZrO_2-Sc_2O_3 system, the phase diagram of the binary system HfO_2-Sc_2O_3 is more complex with respect to others with rare-earth and alkaline-earth metal oxides. In the hafnia-rich part of the HfO_2-Sc_2O_3 system, the three ordered phases $Sc_2Hf_7O_{17}$ (β), $Sc_2Hf_5O_{13}$ (γ), and $Sc_4Hf_3O_{18}$ (δ) exist in addition to the monoclinic, tetragonal, and cubic fluorite solid solutions [58, 60]. Increasing temperature leads to disorder; the temperatures of the $\beta \rightarrow$ F and $\gamma \rightarrow$ F phase transitions were reported to be approximately 953 K and 1123 K, respectively [60]. In the system HfO_2-Y_2O_3, detailed investigations [71] also showed the presence of phases which are not characteristic of pure HfO_2, at yttria concentrations close to the lower stabilization limit of the cubic fluorite phase. In particular, formation of the so-called γ_1 and γ_2 phases having a monoclinically distorted orthorhombic structure was reported at an yttrium oxide concentration of 7 mol% [71].

Among other interesting results regarding hafnia-based ordered phases, one should mention an attempt to predict theoretically the role of oxygen vacancies on phase relationships in the systems HfO_2-Me_2O_3 (Me is rare-earth element) [123].

The binary systems HfO_2-CeO_x and HfO_2-PrO_x, which are of interest from the viewpoint of mixed ionic-electronic conductivity, behave like the corresponding zirconia-based systems [1]. Domains of solid solution based on hafnia M- and T-phases, and cubic ceria-based phases, with two-phase fields between them, were found in the system HfO_2-CeO_2 in oxidizing conditions [89, 90]. No pyrochlore phase is formed with tetravalent cerium cations [89, 90]; the existence of a pyrochlore-type cerium hafnate was found only at high temperatures under vacuum [92]. In contrast to cerium cations, trivalent praseodymium ions can be stabilized when dissolving praseodymium oxide in the hafnia fluorite phase, or forming pyrochlore-type $Pr_2Hf_2O_7$ [93–95]. In the system HfO_2-PrO_x, praseodymium cations were found to be predominantly in the state Pr^{3+} up to concentrations of PrO_x as high as 50 mol%, and only further increase in the praseodymia content leads to formation of Pr^{4+} [93].

Finally, one should note that analogously to the zirconia-based phase diagrams, no new ternary phases form in the hafnia-rich part of the ternary oxide systems. Cubic fluorite solid solutions were found only in ternary systems where the F-phase forms in at least one binary system; in comparison with the binary systems, no enlargement of the fluorite phase stability domain can be obtained by introducing a third metal oxide.

Electrical transport in the fluorite-type HfO_2-based solid solutions

As found for cubic fluorite phases of zirconia stabilized with REE oxides, hafnia-based fluorites exhibit predominant oxygen ionic conductivity; the qualitative dependencies of ionic transport on dopant concentration in HfO_2-based materials are analogous to those found for ZrO_2, considered in the first part of this review [1]. Firstly, the oxygen ionic conductivity in solid solutions of $Hf(Me)O_2$ (with Me a rare-earth element) increases with decreasing ionic radius of dopant cations (Fig. 2). The maximum conductivity is observed for the cubic hafnium dioxide stabilized with scandia, ytterbia, and yttria [61, 65–67, 76–78, 80, 96, 124, 125]. Selected data on conductivity of HfO_2-based solid electrolytes are given in Table 4. Secondly, the maximum conductivity is characteristic of materials containing a minimum amount of stabilizing dopant, when the composition is close to the low stabilization limit of the fluorite phase [61, 65, 66, 78, 106]. Further increase in REE dopant content leads to decreasing conductivity and increasing activation energy for ionic transport. At the same time, it should be noted that references on exact compositions with the highest conductivity show an important scatter in values owing to different processing conditions, slow kinetics of solid-state synthesis, the presence of impurity phases, and the relatively high rate of degradation of the hafnia-based fluorites with time. For instance, the maximum conductivity in the HfO_2-Y_2O_3 system was reported for Y_2O_3 concentrations of 8 mol% [78], 10 mol% [65, 76], and 8–12 mol% [66].

When considering the most important differences between solid electrolytes based on HfO_2 and ZrO_2, one should mention a lower ionic conductivity (see, for example, [77, 126, 127]), higher electronic conduction [67, 98, 128], and higher ageing rate [65, 77] as characteristics of hafnia-based materials. The poor ionic transport properties of hafnia-based materials, illustrated in Figs. 2 and 3, and faster degradation are associated with specific features of the phase diagrams discussed above. The thermodynamic stability at intermediate temperatures of the stabilized HfO_2-based fluorite phases is lower than for stabilized zirconia, and the tendency for partial decomposition and local ordering in the oxygen sublattice of oxides containing moderate amounts of stabilizing additions is more

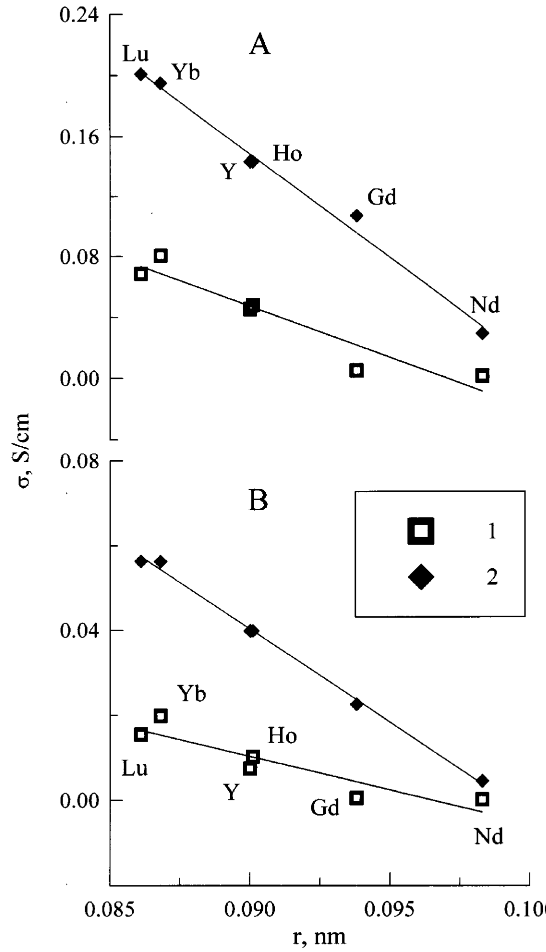

Fig. 2 Dependence of the total electrical conductivity of hafnia (*1*) and zirconia (*2*) stabilized with 10 mol% rare-earth additions, on radius of the REE cations at 1273 K (**A**) and 1073 K (**B**). Data from [96, 151]

important in the case of hafnia. Also, for hafnia-based fluorites, a complete f-shell and a small radius of Hf^{4+} result in small unit cell parameters if compared to those of zirconia (Table 5). All these aspects lead to lower ionic conductivity of $Hf(Me)O_2$ solid solutions with respect to $Zr(Me)O_2$ with the same content of stabilizing dopant (Fig. 2).

The ionic conductivity dependence on ageing of the stabilized-hafnia electrolytes shows similarities to zirconia, but HfO_2-based ionic conductors are characterized by significantly faster degradation with time [77, 129, 130]. Ageing of these materials leads to decreasing oxygen conductivity and increasing activation energy for ionic transport. All electrolytes possess a critical temperature where intensive degradation starts (T_{sd}); at higher temperatures, the ionic conductivity is time-independent. For fluorite-type oxides in the system HfO_2-Y_2O_3, increasing the concentration of stabilizing additions was found to result in higher T_{sd} values [77]; this critical temperature increased from 1270 to 1510 K when the content of Y_2O_3 increased from 10 to 25 mol%. The fast ageing processes of the HfO_2-based

Table 4 Electrical conductivity of HfO_2-based fluorite solid solutions

Composition		Sample[a]	Conductivity, S/cm			Activation energy		Ref.
Dopant	Concentration (mol%)		973 K	1173 K	1373 K	T (K)	E_A (eV)	
HfO_2 (99.3%)		C	–	1.0×10^{-4}	5.6×10^{-4}	1050–1780	1.3	[76]
Y_2O_3	10	C	1.8×10^{-3}	2.0×10^{-2}	4.5×10^{-2}	–	–	[79]
Y_2O_3	10	SC	1.9×10^{-3}	1.5×10^{-2}	5.1×10^{-2}	800–1700	1.2	[124]
Y_2O_3	12.5	C	2.6×10^{-3}	1.3×10^{-2}	–	773–1073	1.1	[66]
Y_2O_3	20	C	3.0×10^{-4}	3.8×10^{-3}	–	773–1223	1.3	[66]
Y_2O_3	20	SC	3.2×10^{-4}	4.3×10^{-3}	1.9×10^{-2}	800–1700	1.7	[124]
Nd_2O_3	10	C	1.1×10^{-4}	1.0×10^{-3}	7.5×10^{-3}	–	–	[98]
Nd_2O_3	15	C	3.1×10^{-4}	2.1×10^{-3}	1.1×10^{-2}	–	–	[98]
Nd_2O_3	20	C	1.9×10^{-4}	1.4×10^{-3}	4.0×10^{-3}	–	–	[98]
Gd_2O_3	9	C	4.0×10^{-4}	4.1×10^{-3}	2.2×10^{-2}	–	–	[106]
Gd_2O_3	13.2	C	2.4×10^{-4}	3.5×10^{-3}	1.9×10^{-2}	–	–	[106]
Gd_2O_3	19.5	C	1.1×10^{-4}	1.7×10^{-3}	1.0×10^{-2}	–	–	[106]
Yb_2O_3	10	C	5.4×10^{-3}	4.4×10^{-2}	0.14	1073–1473	1.5	[79]
Yb_2O_3	10	SC	1.9×10^{-2}	0.10	0.29	1073–1273	1.3	[124]
Dy_2O_3	10	C	2.1×10^{-3}	2.6×10^{-2}	9.8×10^{-2}	1073–1473	1.8	[79]
Ho_2O_3	10	C	2.5×10^{-3}	2.4×10^{-2}	9.0×10^{-2}	1073–1473	1.8	[79]
Tm_2O_3	10	C	3.6×10^{-3}	2.8×10^{-2}	0.11	1073–1473	1.7	[79]
Lu_2O_3	10	C	4.1×10^{-3}	3.6×10^{-2}	0.12	1073–1473	1.5	[79]
Sm_2O_3	10	C	8.7×10^{-4}	1.1×10^{-2}	4.1×10^{-2}	1073–1473	2.0	[79]
Er_2O_3	10	C	2.9×10^{-3}	3.3×10^{-2}	0.11	1073–1473	1.6	[79]

[a] C corresponds to ceramics; SC is the single crystal

solid electrolytes may cause excessively large experimental scatter in conductivity measurements at temperatures below T_{sd} [77].

In oxidizing conditions, the high p-type conductivity of stabilized hafnia with respect to zirconia, estimated from data on the total conductivity as a function of oxygen partial pressure [78, 100], the e.m.f. of oxygen concentration cells [61, 78, 100, 106], and ion-blocking measurements [67, 98], was attributed to the f-shell in hafnium cations and the higher stability of defects in the HfO_2 crystal lattice [98]. Figure 4 shows the temperature dependencies of the total and p-type electronic conductivity for two widely known solid electrolytes based on zirconia and hafnia, illustrating this feature. Note that phase decomposition of the hafnia-based solid solutions, leading to formation of monoclinic hafnia with predominant p-type conductivity, can also increase the role of electronic transport on the total conductivity. Among other $Hf(Me)O_2$ solid solutions, the highest electron transference numbers are typical of ceramics containing variable-valence rare-earth cations (Me = Pr, Nd, Tb) [98, 100]. In all cases, however, the electronic contribution does not exceed 25% of the total conductivity of the fluorite phases. Decomposition of the metastable fluorite $(HfO_2)_{0.85}(Pr_2O_3)_{0.15}$ at 1573 K, to form solid solutions with monoclinic and pyrochlore structures, was reported to cause a dramatic decrease of the ionic conductivity, while the effect of the phase composition on the electronic transport is much weaker [98]. As a result, the electron transference numbers of $(HfO_2)_{0.85}(Pr_2O_3)_{0.15}$ ceramics in high-purity helium increased during decomposition up to 0.90–0.95 [98].

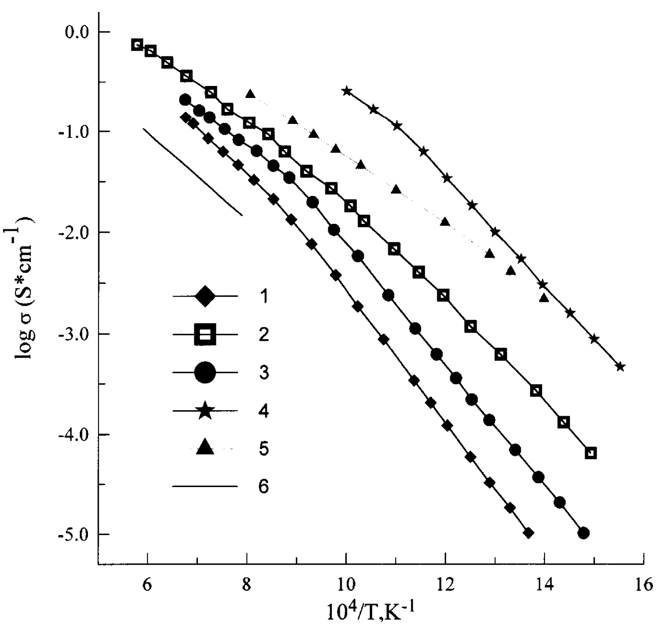

Fig. 3 Temperature dependence of the conductivity of hafnia (*1*, *3*) and zirconia (*2*) stabilized with 10 mol% yttria (*1*, *2*) and ytterbia (*3*) [96, 152]. Data on conductivity of the solid electrolytes $Bi_{0.75}Y_{0.25}O_{1.5}$ [153], $Ce_{0.8}Gd_{0.2}O_{1.9}$ [154], and $Th_{0.85}Y_{0.15}O_{1.925}$ [155] are also presented for comparison (curves *4*, *5*, and *6*, respectively)

Electrical properties of $Me_2Hf_2O_7$ pyrochlores and $Me_4Hf_3O_{12}$ δ-phases

Both pyrochlore and hexagonal δ-phases, being the ordered derivatives of the fluorite structure, possess much lower ionic conduction in comparison with the F-type solid solutions. In the systems HfO_2-Me_2O_3 (Me is

Table 5 Properties of single crystals of yttria-stabilized hafnia and zirconia [67]

Oxide	Y_2O_3 content (mol%)	Cubic lattice parameter a (nm)	Density (kg/m^3)	Microhardness H (GPa)
HfO_2	10	0.5129	9470	21.26
	15	0.5139	9060	17.39
	20	0.5156	8690	16.13
	25	0.5172	8310	15.34
	33	0.5196	7760	14.75
ZrO_2	10.3	0.5141	5910	15.29
	13.8	0.5156	5860	14.12
	19.8	0.5162	5800	13.62
	26.3	0.5190	5655	13.48
	31.2	0.5206	5600	12.76
	25.9	0.5220	5540	12.66

rare-earth element), formation of these phases is accompanied by a sharp minimum in the composition dependence of the conductivity [61, 65, 66, 76, 78, 82–84, 93, 98, 100, 106]. Correspondingly, disorder and transition to the fluorite phase with increasing temperature causes a drastic increase in the total conductivity and ionic transference numbers of the oxide materials. Thermal expansion coefficients and values of the total electrical conductivity of selected hafnates are listed in Tables 2 and 3. Thermodynamic properties of the REE pyrochlores have been reported [131]. Results on the crystal structure and physical properties of $La_2Hf_2O_7$, including thermal expansion, have also been presented [132].

In oxidizing conditions, the pyrochlore-type hafnates exhibit a mixed oxygen ionic and p-type electronic conductivity [84, 98, 100]. Their total conductivity decreases with reducing oxygen pressure down to 10^{-2}–10^{-3} Pa, changing linearly with $p(O_2)^{1/4}$. At oxygen partial pressures close to that in air and temperatures

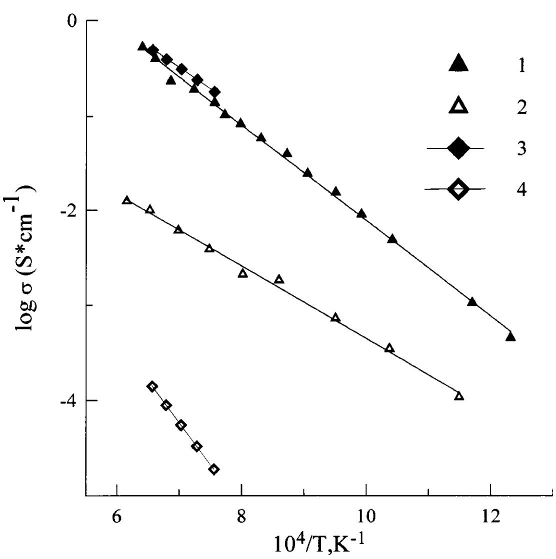

Fig. 4 Temperature dependence of total (*1*, *3*) and p-type electronic (*2*, *4*) conductivities of fluorite phases consisting of 10 mol% yttria doped hafnia (curves *1* and *2*) and zirconia (curves *3* and *4*). Data from [67, 156]. The electronic conductivity of the stabilized hafnia electrolyte was measured by the ion-blocking technique, in vacuum [67]. The electronic conductivity of zirconia was calculated from the total conductivity and oxygen permeation data [156]

from 970 to 1770 K, the ion transference numbers of $Me_2Hf_2O_7$ (Me = La, Pr, Nd) are less than 0.2 [84, 98, 100]. The total conductivity of $La_2Hf_2O_7$ in the oxygen pressure range from 10^{-4} to ca. 10^{-10} Pa is predominantly ionic [84]; for $Pr_2Hf_2O_7$, the p-type electronic conduction was reported to be predominant even in high-purity helium [98]. In the case of $Gd_2Hf_2O_7$, ion transference numbers as high as 0.4–0.6 in oxygen were estimated by the e.m.f. method [106].

Analogously to the pyrochlore-type zirconates, introduction of hyperstoichiometric amounts of rare-earth cations into the pyrochlore lattice of hafnates, within the homogeneity range, forming the solid solutions $Me_2(Hf,Me)_2O_{7-\delta}$, leads to an increase in oxygen vacancy concentration and, therefore, ionic conductivity [84, 98, 100]. The electron hole conductivity also increases with increasing rare-earth oxide content, caused probably by incorporation of oxygen in the formed oxygen vacancies; as a consequence, the transference numbers do not change significantly within the limits of solid solutions with the pyrochlore structure [84, 100, 106].

The δ-phases, $Me_4Hf_3O_{12}$ (Me = Sc, Er-Lu), were reported to be dielectric at room temperature [62]. These compounds, with Me = Er, Tm, and Yb, exhibit paramagnetic properties at 78–293 K [17]. Increasing temperature results in mixed ionic-electronic conduction, whereas after the $\delta \rightarrow$ F transition the conductivity increases by 10–100 times, and becomes predominantly ionic [17, 62]. The $\delta\leftrightarrow$F phase transformation leads to a broad hysteresis in the conductivity versus temperature curves. Metastable fluorite-type solid solutions, which can be obtained by quenching, have a significantly higher ionic conduction in comparison to the δ-phases [62]. As found for $Me_4Zr_3O_{12}$ [1], the mixed conductivity of the $Me_4Hf_3O_{12}$ ceramics increases with increasing radius of REE cations [17, 62], demonstrating thus an opposite behavior with respect to the fluorite phases. Seebeck coefficient studies [62] showed that the electronic conduction in the hafnia-based δ-phases in air, at temperatures below 900–1070 K, is n-type, in contrast to the pyrochlores and fluorites. Further increase in temperature leads to an increasing role of oxygen vacancy migration in the electrical conductivity [62]. IR spectra of $Me_4Zr_3O_{12}$ compounds have been studied [133].

Processing and reactivity of HfO_2-based ceramics

Numerous research projects [2, 24, 80, 85, 99, 125, 134–144] focused on solid-state synthesis mechanisms, development and optimization of processing conditions, and on the role of the preparation route on properties of hafnia-containing materials. These materials were considered not only for possible electrochemical applications, but also as promising refractories and dielectrics. Interaction of hafnia with other refractory metal oxides such as TiO_2 [115, 143], Cr_2O_3 [144], Al_2O_3 [74, 113, 114, 145], Ta_2O_5 [146], and In_2O_3 [147], and corresponding phase diagrams, were studied in detail. Generally, the formation mechanisms of the hafnia-based cubic fluorite phases are similar to those found for zirconia [85, 134]. In the HfO_2-Me_2O_3 systems (Me is rare-earth element), formation of the F-phases occurs via diffusion of rare-earth metal cations with subsequent incorporation into the hafnia crystal lattice [134, 139]. For HfO_2-CaO, the fluorite phase forms via the more stable $CaHfO_3$ perovskite phase [24], as found for the system ZrO_2-CaO [1]. At the same time, the solid-state synthesis of hafnia-based solid electrolytes requires higher temperatures with respect to zirconia, as can be expected from the phase diagrams. The temperature required for solid-state reactions involving hafnia can be reduced by partial substitution of HfO_2 with ZrO_2 [80, 85]. For instance, the minimum temperature necessary to obtain a single fluorite phase stabilized by yttria, ytterbia, or gadolinia was 1770 K for the $0.65HfO_2 + 0.35ZrO_2$ mixture. This is significantly lower than found for hafnium dioxide without zirconia additions [80]. The synthesis temperatures can also be reduced decreasing the size of particles in the starting mixtures for solid-state reactions [136], or using techniques such as co-precipitation or decomposition of organometallics [148, 149]. Among the most interesting results, one should mention a significant enlargement of the apparent solid solubility domains in the ceramics of HfO_2-Me_2O_3 (Me = La-Lu, Y) obtained by shock-wave synthesis [137].

Hafnia-based oxide materials exhibit significantly better mechanical properties and chemical stability than zirconia (see, for example, [2, 67, 125]). In particular, the microhardness of single crystals of fluorite-type $Hf(Y)O_2$ is 15–30% higher than that of $Zr(Y)O_2$ solid solutions (Table 5). Testing of the thermal properties of yttria-stabilized hafnia ceramics showed that the thermal-shock resistance can be improved by additions of Al_2O_3 and $MgAl_2O_4$ [125]. The optimum stability was found for addition of 1 mol% of the aluminum-magnesium spinel [125]. Comparative tests of the corrosion of the stabilized ZrO_2 and HfO_2 ceramics in vapors and melts of alkaline metals [125] demonstrated the considerably higher stability of hafnia (Table 6). These features may be useful for possible applications of hafnia-based solid electrolytes as electrochemical sensors for the measurement of oxygen concentration in melted metals, at relatively high temperatures, when the ionic conductivity of stabilized HfO_2 is sufficient.

Ceramic materials based on cerium dioxide

Ionic and mixed ionic-electronic conductors based on doped CeO_2 attracted more interest for electrochemical applications than those based on stabilized hafnia, owing to their higher oxygen ionic conductivity (see, for instance, Fig. 3). Doped CeO_2 materials can be considered as promising solid electrolytes for SOFCs operating at temperatures below 970 K. At the same time, ceria-based oxides possess some specific disadvantages. The main disadvantages are dimensional instability and mechanical decomposition at temperatures above 1000–1050 K in reducing environments, where the reduction of cerium dioxide and the transition $CeO_2 \rightarrow CeO_{1.5}$ take place. Another specific feature of doped ceria is the appearance of significant n-type electronic conductivity at low oxygen partial pressures. While the electronic conductivity can be suppressed by an appropriate choice of operating conditions or dopants, the mechanical decomposition of the solid electrolyte ceramics is an irreversible process. This instability is often observed in electrochemical cells using reducing gases. Providing absolutely uniform distributions of temperature and oxygen chemical potentials in large solid electrolyte cells is a complex engineering task, and local overheating and reduction of the solid electrolyte ceramics may often take place. As a result, the applicability of doped CeO_2 solid electrolytes in cells such as SOFCs and high-temperature electrolyzers is limited [148].

As found for the solid electrolyte materials, the use of mixed-conducting ceria-based ceramic membranes for partial oxidation of hydrocarbons is also limited by the possible mechanical decomposition in reducing environments, at high temperature. In the case of membranes, another limiting factor is a relatively low electronic conductivity of ceria doped with variable-valence metal oxides, which is associated with a low solid solubility of such dopants in the fluorite-type cerium dioxide lattice, analogously to zirconium dioxide ceramics [1].

The advantages of ceria-based materials include a high oxygen ionic conductivity, relatively low TECs, and a very high catalytic activity with respect to oxidation reactions. This feature caused a considerable interest for

Table 6 Stability of stabilized zirconia and hafnia ceramics with respect to alkaline metals [125]

Composition (mol%)	Weight loss after testing in melted alkaline metal at 873 K for 10 h (%)	Corrosion rate in Na vapor at 773 K (mg cm^{-2} h^{-1})
$85ZrO_2 + 15CaO$	100	0.09
$94ZrO_2 + 6Y_2O_3$	100	–
$90ZrO_2 + 10Y_2O_3$	100	–
$85HfO_2 + 15CaO$	100	0.0275
$90HfO_2 + 10Y_2O_3$	41	0.014
$50HfO_2 + 50Y_2O_3$	18	0.003

electrocatalytic applications, including anodes for SOFCs and activating additions to electrode materials operating in reducing atmospheres [1, 148].

When reviewing the literature on CeO_2 published in the former Soviet Union, one should mention an excellent monograph by Leonov [157], where a detailed analysis of the properties of cerium oxides and compounds with other metal oxides was presented. Properties of CeO_2-based solid electrolytes were also briefly analyzed in other monographs [148, 158].

Properties of cerium dioxide

In contrast to undoped zirconium and hafnium dioxides, pure CeO_2 exhibits no phase transitions in oxidizing conditions up to the melting point. The cubic fluorite phase is the only stable phase in the system Ce–O at high oxygen pressures [157]. At temperatures below 1700 K in air, oxygen nonstoichiometry in ceria is relatively small [157]. As a result, the concentration of defects determining the transport properties of ceria depends strongly on history and impurity content (Tables 7 and 8). Undoped CeO_2 is a mixed ionic and n-type electronic conductor in air [159–166]. The electronic conductivity occurs via a small polaron mechanism and increases proportional to $p(O_2)^{-1/4}$ at moderate oxygen pressures [159, 160, 163, 165, 166]. Reducing the cerium dioxide content leads to decreasing activation energy for electronic transport, which was explained in terms of decreasing Coulombic interaction between the defects of the fluorite lattice [167]. For instance, the activation energies for total conductivity were reported to be approximately 96 and 41 kJ/mol for $CeO_{2.00}$ and $CeO_{1.90}$, respectively, whereas the conductivity of oxygen-deficient $CeO_{1.90}$ was reported to be higher than that of stoichiometric ceria by several orders of magnitude [160]. Owing to partial reduction, the conductivity of as-prepared single crystals of cerium dioxide significantly exceeds the corresponding values for samples annealed in air (Table 7). A detailed analysis of the electronic transport in $CeO_{2-\delta}$ as a function of oxygen pressure, temperature, and impurity content has been performed [165–167].

Ionic conduction in $CeO_{2-\delta}$ is determined mainly by two factors: concentration of vacancies in the oxygen sublattice and their association with impurity cations [159, 164, 167]. Incorporation of moderate amounts of impurity cations with oxidation state lower than 4+ leads to a sharp increase in oxygen conductivity and activation energy for ionic transport. For example, the oxygen diffusion coefficient in single crystals of cerium dioxide containing 0.3 at% gadolinium oxide was found to be higher than the oxygen diffusivity in "undoped" crystals (gadolinia content of $\sim 3 \times 10^{-5}$ at%), by a factor of 5–1000, at 1000–1600 K [168]. The temperature dependencies of the diffusion coefficients can be approximated by the equations

$$D_O = 9.55 \times 10^{-5} \exp\left(-\frac{0.94\,\mathrm{eV}}{kT}\right) \tag{2}$$

$$D_O = 5.34 \times 10^{2} \exp\left(-\frac{3.17\,\mathrm{eV}}{kT}\right) \tag{3}$$

for the 0.3 at% gadolinia-doped and "undoped" samples, respectively, with D_O expressed in $cm^2\ s^{-1}$. As a result of the drastic dependence of ionic conduction on dopant content, decreasing sample purity leads to increasing oxygen ion transference numbers (Table 8). The effect of reducing oxygen partial pressure on ionic

Table 7 The total conductivity of cerium dioxide

Samples and purity[a]	Pre-history	Conductivity (S/cm)			Activation energy		Ref.
		523 K	1073 K	1323 K	T (K)	E_A (eV)	
C (97.5%)	After sintering at 1823 K in air	–	2.0×10^{-3}	1.7×10^{-2}	1073–1423	1.0 (ionic) 2.3 (electronic)	[159]
C (99.7%)	After sintering at 1773 K in air	1.0×10^{-7}	8.0×10^{-3}	4.7×10^{-2}	–	–	[160]
C (99.7%)	After sintering at 1573 K in air	5.9×10^{-11}	3.4×10^{-4}	5.0×10^{-3}	513–1573	2.68	[161]
SC (99.9%)	After preparation from salt melting	8.7×10^{-3}	0.13	–	293–1273	0.24	[162]
SC (99.9%)	After annealing at 1473–1573 K in air	3.0×10^{-10}	1.6×10^{-3}	1.1×10^{-2}	293–1273	1.28	[162]

[a] C corresponds to ceramics; SC is the single crystal

Table 8 Oxygen ion transference numbers of ceria calculated from data on the oxygen partial pressure dependence of total conductivity

Purity	Oxygen pressure $p(O_2)$ (atm)	Ion transference numbers, t_O				Ref.
		1073 K	1173 K	1273 K	1373 K	
97.5%	1.0	1.00	0.95	0.89	0.68	[159]
	0.21	1.00	0.94	0.87	0.61	
	1.0×10^{-2}	1.00	0.89	0.74	0.44	
99.5%	1.0	0.91	0.78	0.59	0.35	[163]
	0.21	0.89	0.69	0.45	0.25	
	1.25×10^{-2}	0.76	0.50	0.26	0.14	
	5×10^{-4}	0.66	0.31	0.14	0.06	

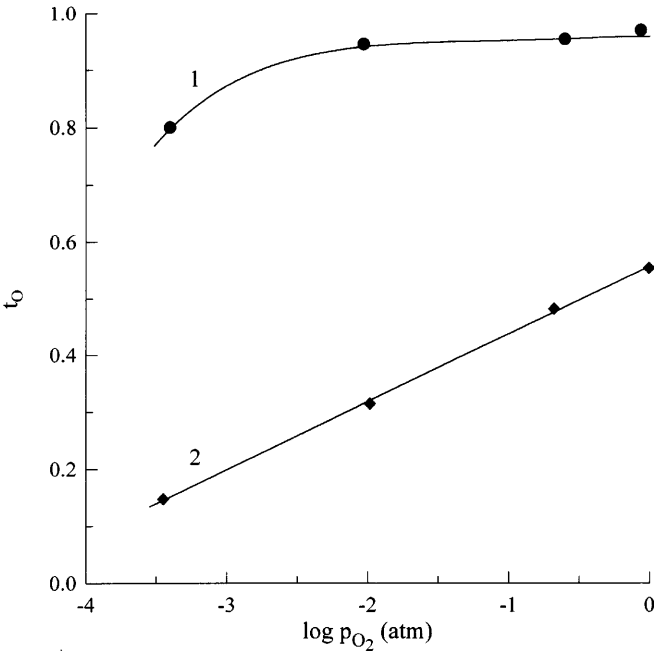

Fig. 5 Temperature dependence of the $CeO_{2-\delta}$ oxygen ion transference number calculated from results of total conductivity as a function of oxygen partial pressure [159]: *1*, 1123 K, *2*, 1423 K

transport is more complex, probably due to trapping of oxygen vacancies. In particular, a decrease in ionic conductivity with reduction has been mentioned in ceria single crystals [164], while the oxygen diffusion coefficient estimated from the creep behavior of ceramic samples was reported to increase with increasing vacancy concentration [160]. The temperature dependencies of oxygen ion transference numbers of nonstoichiometric ceria (Fig. 5) are determined by the activation energies for ionic and n-type electronic transport. When the oxygen deficiency is relatively small, the activation energy for electronic conduction is higher, and the values of t_O decrease with temperature [159, 163], whereas the behavior in reducing conditions is the opposite [163].

Along with the transport properties [157, 159–168], numerous research projects have focused on thermodynamic [169–173] and catalytic [174–177] properties of phases in the Ce–O system as well as an their EPR spectra [178, 179]. The oxygen exchange of cerium dioxide with the gas phase is considered below. When reviewing other results interesting for high-temperature electrochemical applications, one should consider the formation of superstructures in the cerium dioxide lattice when oxygen deficiency increases [173]. Reduction of $CeO_{2-\delta}$ into Ce_2O_3 occurs via formation of a series of discrete phases, which can be represented as [173]:

$$CeO_2 \rightarrow CeO_{1.87} \rightarrow CeO_{1.75} \rightarrow CeO_{1.62} \rightarrow CeO_{1.5} \qquad (4)$$

Thermodynamic characteristics of Ce-O phases were studied in detail [172]. Thermal expansion coefficients of cerium dioxide and selected ceria-based oxide compounds are listed in Table 9.

Phase relationships in the systems CeO_2-MO and CeO_2-Me_2O_3

Since ionic transport properties of ceria are determined by the concentration of oxygen vacancies which can be created by incorporation of lower-valence cations into the crystal lattice, the CeO_2-MO (M is alkaline-earth element) and CeO_2-Me_2O_3 (Me is rare-earth element) oxide systems have attracted considerable interest as potential solid electrolyte materials.

Selected phase relationships and crystal structures of separate oxide phases were studied in the systems CeO_2-BeO [183–185], CeO_2-MgO [180, 183–186], CeO_2-CaO [180, 183–185, 187–189], CeO_2-SrO [180, 183–185, 188, 190–192], and CeO_2-BaO [183, 185, 188, 193]. In the binary CeO_2-MO (M = Be, Sr, Ba) systems, the fluorite-type solid solution concentration ranges are very narrow. In particular, the solid solubility of barium cations in ceria, at 1270–1770 K, does not exceed 2 mol% of BaO [193]. However, the solid solubility in these three systems cannot be considered as irrelevant. In fact, small

Table 9 Thermal expansion coefficients of CeO_2-based oxides[a]

Composition	Method	Average TEC values				Ref.
		T (K)	$\bar{\alpha} \times 10^6$ (K^{-1})			
CeO_2	XRD	293–1073	6.25			[180]
$Ce_{0.9}Gd_{0.10}O_{2-\delta}$	D	300–1100	8.2			[181]
$Ce_{0.88}Co_{0.02}Gd_{0.10}O_{2-\delta}$	D	300–1100	11.17			[181]
$Ce_{0.80}Co_{0.10}Gd_{0.10}O_{2-\delta}$	D	300–1100	11.9			[181]
$(CeO_2)_{0.91}(SrO)_{0.09}$	XRD	293–1213	11.80			[180]
			$\alpha_a \times 10^6$ (K^{-1})	$\alpha_b \times 10^6$ (K^{-1})	$\alpha_c \times 10^6$ (K^{-1})	
$SrCeO_3$		298–1773	11.2	9.2	7.6	[182]
$Sr(Ce_{0.75}Zr_{0.25})O_3$	X-ray	298–1773	10.7	8.6	8.4	[182]
$Sr(Ce_{0.50}Zr_{0.5})O_3$		298–1773	9.8	8.2	9.5	[182]

[a] D is the dilatometric method; XRD is the high-temperature X-ray diffraction technique; α_a, α_b, and α_c are the TECs for the *a*-, *b*-, and *c*-axis of the crystal lattice, respectively

additions of barium, magnesium, and beryllium oxides result in considerably high conductivities of two-phase ceramics containing the ceria-based cubic fluorite phase and BeO, MgO, or $BaCeO_3$ with respect to undoped ceria, owing to formation of oxygen vacancies with such additions [183, 185]. The concentration range of the single fluorite phase in the systems CeO_2-CaO and CeO_2-SrO is wider and reaches up to 15–20 mol% at 1870–2070 K. Decreasing temperature leads to a drastic decrease in the solubility of calcium and strontium oxides [186, 194]. For instance, the maximum concentration of SrO in the $Ce(Sr)O_{2-\delta}$ solid solutions was 8 mol% at 1200–1400 K [190]. Notice that the decomposition process of $Ce(M)O_{2-\delta}$ solid solutions, which are metastable at low temperature, is relatively slow. This causes some disagreement in the literature with regard to the concentration ranges of solid solution formation.

In the systems CeO_2-SrO and CeO_2-BaO, $MCeO_3$ perovskite-like cerate phases are formed [180, 183–185, 188, 190–194]. The thermodynamic stability of cerates is significantly smaller than for perovskite-type hafnates and zirconates [193]. Formation of calcium cerate is generally unfavorable from thermodynamic and structural viewpoints [187]. Barium and strontium cerates are, however, more stable in the CeO_2-MO systems than the $Ce(M)O_{2-\delta}$ fluorites [190, 193]. As a result, in the course of solid-state synthesis, formation of fluorite-type $Ce(Sr)O_{2-\delta}$ occurs via intermediate formation of the $SrCeO_3$ perovskite [192], as found for the systems of zirconium and hafnium dioxides with alkaline-earth metal oxides.

The solid solubility of rare-earth cations in the cerium dioxide fluorite-type lattice is considerably higher if compared to the alkaline-earth metals [180, 194–196]. For example, the maximum concentrations of $LaO_{1.5}$, $NdO_{1.5}$, and $YO_{1.5}$ in $Ce(Me)O_{2-\delta}$ solid solutions, synthesized by solid-state reaction in air at 1820 K, were reported to be 40–45, 60, and 35 mol%, respectively [180]. No phase decomposition takes place at low temperature. The higher solid solubility of REE cations in ceria as well as a significantly better thermodynamic stability of the $Ce(Me)O_{2-\delta}$ fluorites makes the CeO_2-Me_2O_3 oxide systems much more promising for electrochemical applications than CeO_2-MO solid solutions.

The sinterability and solid-state synthesis of ceria-based ceramic materials were also studied in detail [192, 197, 198].

Electrical conduction in the CeO_2-based fluorite phases

All the fluorite-type phases based on cerium dioxide have predominant oxygen ionic conductivity in oxidizing conditions [167, 183, 185, 195, 196]. The electronic contribution to the total conductivity in air may be both n- or p-type, depending on concentration of dopants. In particular, an increase in p-type electronic conduction with increasing neodymia content was found in the CeO_2-Nd_2O_3 ceramics with high concentrations of Nd_2O_3 [196]. Moderate addition of both rare-earth and alkaline-earth metal oxides results in increasing randomly distributed oxygen vacancies and, correspondingly, oxygen ionic conductivity. For the REE-doped ceria, the maximum ionic conduction in the $Ce_{1-x}Me_xO_{2-\delta}$ solid solutions corresponds to values of x from 0.15 to 0.20 [148, 167, 195]. Further addition of rare-earth dopants leads to decreasing ionic transport and increasing activation energy for oxygen conductivity owing to an increasing role of defect association (oxygen vacancies and impurity cations). In the case of alkaline-earth metal oxide additions, the maximum ionic transport is observed for ceramics containing 10–15 mol% dopant [183, 185]. Here, decrease in conductivity with increasing dopant content is caused not only by defect association, but also by decomposition of $Ce(M)O_{2-\delta}$ solid solutions, metastable at low temperatures. As found for oxide systems with zirconia and hafnia, segregation of the $MCeO_3$ perovskite-type cerate phases, having low mixed p-type electronic and ionic conductivity in air [15, 185, 200, 201], leads to a sharp decrease in the conductivity of the CeO_2-MO ceramics [183, 185, 191].

Selected data on the conductivity of CeO_2-based ceramics in air and ionic transference numbers, estimated from oxygen concentration cell e.m.f. measurements and conductivity dependence on oxygen partial pressure, are listed in Table 10. Note that the values of the transference numbers may be underestimated with respect to their true values owing to non-negligible electrode polarization [199], porosity of the ceramics [196], other experimental constraints of the e.m.f. method [158, 199], and dependence of ionic conductivity of ceria on oxygen pressure.

Analogously to undoped $CeO_{2-\delta}$, the n-type conductivity and activation energy for electronic transport in ceria-based solid solutions increases drastically with reducing oxygen chemical potential in the gas phase. Such behavior was studied in detail using ceramics of $Ce_{1-x}La_xO_{2-\delta}$ ($x = 0$–0.62) as a model system [167]. It was found that both electronic conductivity and reducibility, expressed by the concentration of trivalent cerium cations, correlates with the dopant content in the $Ce(La)O_{2-\delta}$ solid solutions, having a maximum at 15–20 mol% of lanthanum oxide (Figs. 6 and 7). Taking into account that the maximum ionic conductivity is also characteristic of this range of x [195], one can conclude that both ionic conduction and reducibility of ceria-based oxides are determined by the fluorite lattice chemical bonding characteristics.

The oxide system CeO_2-ZrO_2

The binary CeO_2-ZrO_2 [204, 205] and ternary CeO_2-ZrO_2-CaO [202, 206] systems were considered as possible alternative solutions to improve the properties of both zirconia and ceria solid electrolytes, namely to increase the ionic conductivity of stabilized ZrO_2 and to suppress

Table 10 Total conductivity and oxygen ion transference numbers of CeO_2-based ceramics in air

Composition	σ (S/cm)		Ref.	t_O 1273 K	Ref.
	873 K	1273 K			
$(0.75CeO_2 \cdot 0.25ZrO_2)_{0.92}(CaO)_{0.08}$	–	4.7×10^{-3}	[202]	0.699	[202]
$(0.75CeO_2 \cdot 0.25ZrO_2)_{0.875}(CaO)_{0.125}$	–	1.5×10^{-2}	[202]	0.899	[202]
$(0.75CeO_2 \cdot 0.25ZrO_2)_{0.81}(CaO)_{0.19}$	–	2.3×10^{-2}	[202]	0.960	[202]
$(0.75CeO_2 \cdot 0.25ZrO_2)_{0.60}(CaO)_{0.40}$	–	3.4×10^{-2}	[202]	0.991	[202]
$(CeO_2)_{0.95}(CaO)_{0.05}$	2.2×10^{-4}	6.0×10^{-3}	[183]	–	
$(CeO_2)_{0.90}(CaO)_{0.10}$	4.7×10^{-4}	1.5×10^{-2}	[183]	–	
$(CeO_2)_{0.85}(CaO)_{0.15}$	8.3×10^{-4}	2.4×10^{-2}	[183]	0.988	[185]
$(CeO_2)_{0.80}(CaO)_{0.20}$	6.9×10^{-4}	1.6×10^{-2}	[183]	–	
$(CeO_2)_{0.95}(SrO)_{0.05}$	8.5×10^{-5}	9.3×10^{-3}	[183]	0.995	[185]
$(CeO_2)_{0.90}(SrO)_{0.10}$	1.0×10^{-3}	2.2×10^{-2}	[183]	–	
$(CeO_2)_{0.85}(SrO)_{0.15}$	5.0×10^{-3}	6.4×10^{-2}	[183]	0.993	[185]
$(CeO_2)_{0.80}(SrO)_{0.20}$	4.4×10^{-3}	5.8×10^{-2}	[183]	–	
$SrCeO_3$	3.8×10^{-7}	1.4×10^{-5}	[183]	0.940	[185]
$(CeO_2)_{0.95}(BaO)_{0.05}$	1.3×10^{-4}	3.7×10^{-3}	[183]	–	
$(CeO_2)_{0.90}(BaO)_{0.10}$	3.2×10^{-4}	5.5×10^{-3}	[183]	–	
$(CeO_2)_{0.85}(BaO)_{0.15}$	3.0×10^{-4}	4.3×10^{-3}	[183]	0.721	[185]
$BaCeO_3$	3.9×10^{-7}	4.8×10^{-5}	[183]	–	
$(CeO_2)_{0.905}(LaO_{1.5})_{0.095}$	4.5×10^{-3}	5.6×10^{-2}	[195]	0.992	[196]
$(CeO_2)_{0.739}(LaO_{1.5})_{0.261}$	3.1×10^{-3}	8.0×10^{-2}	[195]	0.990	[196]
$(CeO_2)_{0.60}(LaO_{1.5})_{0.40}$	1.8×10^{-3}	8.7×10^{-2}	[195]	0.903	[196]
$(CeO_2)_{0.739}(NdO_{1.5})_{0.261}$	4.8×10^{-3}	7.8×10^{-2}	[195]	0.927	[196]
$(CeO_2)_{0.60}(NdO_{1.5})_{0.40}$	1.8×10^{-3}	0.10	[195]	0.883	[196]
$(CeO_2)_{0.739}(YO_{1.5})_{0.261}$	1.7×10^{-3}	5.7×10^{-2}	[195]	0.921	[196]
$(CeO_2)_{0.60}(YO_{1.5})_{0.40}$	3.7×10^{-4}	3.7×10^{-2}	[195]	0.898	[196]
$Ce_{0.88}Gd_{0.10}Co_{0.02}O_{2-\delta}$	–	0.48	[181]	–	
$Ce_{0.80}Gd_{0.10}Co_{0.10}O_{2-\delta}$	4.2×10^{-3}	0.13	[181]	–	
$Ce_{0.75}Gd_{0.20}Mn_{0.05}O_{2-\delta}$	–	5.3×10^{-2}	[203]	–	
$Ce_{0.70}Gd_{0.20}Mn_{0.10}O_{2-\delta}$	1.2×10^{-2}	0.23	[203]	–	

the reducibility of $CeO_{2-\delta}$. However, doping cerium dioxide with zirconia is ineffective in terms of the target properties. The solid solubility of zirconium cations in the crystal lattice of $CeO_{2-\delta}$ is significant only at high temperatures, achieving up to 76 mol% of ZrO_2 at 2200–2300 K [207]. This range dramatically narrows

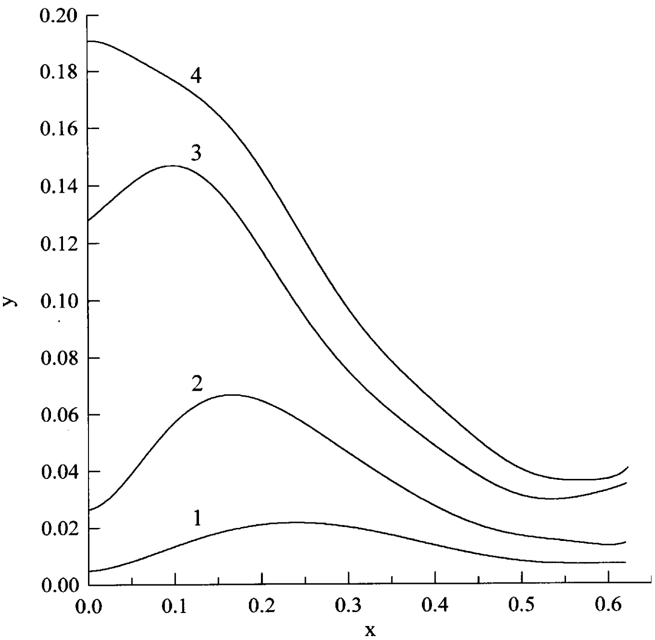

Fig. 6 Dependence of the reducibility of $Ce_{1-x}La_xO_{2-0.5(x+y)}$ solid solutions, expressed as fraction of Ce^{3+} cations in the cerium sublattice (y), on the lanthanum content, in a CO (66 vol%) + CO_2 (34 vol%) gas mixture: *1* 873 K; *2* 1073 K; *3* 1273 K; *4* 1373 K. Data from [167]

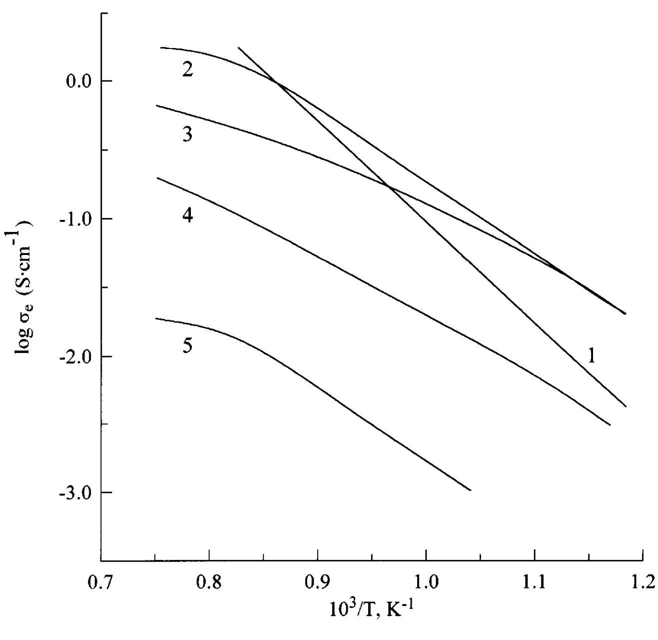

Fig. 7 Temperature dependence of n-type electronic conductivity of solid solutions $Ce_{1-x}La_xO_{2-0.5(x+y)}$ [167] in a CO (66 vol%) + CO_2 (34 vol%) gas mixture. Concentrations of $LaO_{1.5}$: *1* 1.50 mol%; *2* 3.92 mol%; *3* 18.18 mol%; *4* 40.0 mol%; *5* 62.07 mol%

with decreasing temperature and becomes less than 10 mol% at 1270 K. Addition of monoclinic zirconia up to 12 mol% to the ceria cubic phase was found to increase the total conductivity, in the temperature range 770–1520 K [204]. The conductivity of these ceramics is predominantly electronic, as found for undoped ceria and zirconia dioxides. The ionic transference numbers of such materials are less than 0.01 [204]. Analogously to the binary CeO_2-CaO and ZrO_2-CaO systems [1], the ternary CeO_2-ZrO_2-CaO solid solutions are metastable at low temperatures. Introduction of calcium into the zirconia-ceria ceramics increases the ionic conductivity (Table 10) but, because of instability, these oxides cannot operate at temperatures below 1500 K.

Phase relationships in Ce_2O_3-based oxide systems

As mentioned above, one of the most promising applications of cerium-containing oxides refers to anode materials for SOFCs and high-temperature gas electrolyzers, owing to the high catalytic and electrocatalytic activity of cerium cations. Under typical anode conditions, cerium ions are expected to be partly reduced to the trivalent state. Thus, this review includes a short list of references on properties of Ce^{3+}-containing oxide phases, providing information which might be useful for the development of anode materials.

Phase diagrams, separated phase relationships, crystal structures, and properties of selected oxides were reported for the systems Ce_2O_3-MgO [208, 209], Ce_2O_3-Al_2O_3 [210], Ce_2O_3-CaO [208, 211], Ce_2O_3-SrO [208, 212], Ce_2O_3-BaO [208, 213], Ce_2O_3 (CeO_2)-TiO_x [214–219], Ce_2O_3-FeO [220], Ce_2O_3-ZrO_2 [221, 222], Ce_2O_3-Ta_2O_5 [223], Ce_2O_3-WO_3 [224], Ce_2O_3-EuO [225], and Ce_2O_3-TiO_2-Nb_2O_5 [226]. The monographs [157, 227] were devoted to a detailed analysis of some of these oxides, including Ce_2O_3 and perovskite-related compounds containing Ce^{3+}. As a general rule, the phase relationships in oxide systems containing Ce_2O_3 are similar to those in systems with other rare-earth elements having an ionic radius close to Ce^{3+}. In particular, formation of the pyrochlore $Ce_2Zr_2O_7$, which may take place under typical SOFC anode conditions, is observed in the system Ce_2O_3-ZrO_2 [221, 222]. This phase exists only in reducing conditions and is less stable if compared to other trivalent cerium compounds such as $Ce_2Ti_3O_{8.4}$, $Ce_2Si_2O_7$, $CeCrO_3$, or $CeAlO_3$ [221]. Increasing oxygen pressure results in a rapid decomposition of $Ce_2Zr_2O_7$ into two solid solutions based on ZrO_2 and CeO_2. For anode materials for high-temperature electrochemical cells, the perovskite-type $CeTiO_{3\pm\delta}$ and $Ce_{2/3+x}TiO_{3\pm\delta}$ phases [215–217, 227] may be of considerable interest. These perovskites possess a high n-type electronic conductivity in reducing environments. For example, the conductivity of $CeTiO_{3\pm\delta}$ in hydrogen was observed to be temperature-independent at 300–1170 K and to have an order of magnitude of $\sim10^2$ S/cm [227], whereas the presence of the Ce^{3+}/Ce^{4+} redox pair may suggest interesting electrochemical properties for the perovskite-type cerium titanate.

Fluorite-type oxides based on ThO_2

When reviewing data on ThO_2-based solid electrolytes published in the former Soviet Union, one should mention that the total number of open publications in this field is drastically smaller than for research articles regarding other oxygen ionic conductors. This is due to the significant radioactivity of ThO_2-containing oxides. In fact, most research projects concerning radioactive materials in the former USSR were confidential. For instance, the only available publications on phase relationships in ThO_2-containing systems and on crystal structure of selected phases, found by the authors, refer to the ThO_2-MO systems (M = Be, Mg, Ca, Sr, Ba) [180, 228–230], ThO_2–$M'O_3$ oxide phases (M′ = W, Mo), and their compounds with yttria or alkaline metal oxides [231–234], ThO_2–NdOF [235], and ThO_2–$CaCl_2$ [236]; brief data on $Th(Me)O_{2-\delta}$ (Me = Y, La), prepared by the standard ceramic synthesis route, have also been published [237, 238]. Comparison of this small number of publications on ThO_2 with more than 500 articles concerning ZrO_2 and HfO_2 shows that the set of results on thorium dioxide-based materials is incomplete and uncoordinated. Hence, this part of the review only lists data which may still be of interest for oxygen electrochemistry. A brief analysis of the properties of ThO_2-based solid electrolytes and, in particular, their applicability for thermodynamic research is available [158, 239–241].

Generally, while properties of hafnia are close to those of zirconia, the phase relationships and properties of materials in ThO_2-based systems are similar to their equivalents based on CeO_2, owing to the similar electronic structure of thorium and cerium cations. As found for CeO_2, thorium dioxide possesses a cubic fluorite-type structure up to the melting temperature. Data on the solid solubility of alkaline-earth cations in the lattice of ThO_2 [180, 228, 230] are similar to the results on CeO_2, discussed above. For example, the fluorite solid solution concentration ranges in ThO_2-MO systems (M = Be, Mg, Ba) were reported to be quite narrow but not negligible [228]. Calcium and strontium oxides exhibit a higher solid solubility in the thoria fluorite phase, which, however, strongly depends on temperature and preparation conditions [180, 228–230]. Most of the aspects typical of oxygen ionic conduction in ThO_2-based ceramics [158, 228, 237–241] are similar to those observed with cerium dioxide-based materials. The values of total conductivity of some thoria-based ceramics are listed in Table 11.

The main differences in transport properties between thoria and ceria solid electrolytes are similar to the differences between hafnia and zirconia ceramics, mentioned above. Namely, thoria-based electrolytes have

Table 11 Total conductivity of ThO_2-based ceramics in air

Composition	Conductivity (S/cm)		Ref.
	973 K	1273 K	
$(ThO_2)_{0.90}(MgO)_{0.10}$	8.0×10^{-6}	5.8×10^{-4}	[228]
$(ThO_2)_{0.90}(CaO)_{0.10}$	1.5×10^{-5}	6.8×10^{-4}	[229]
$(ThO_2)_{0.85}(CaO)_{0.15}$	1.5×10^{-5}	5.6×10^{-4}	[229]
$(ThO_2)_{0.90}(SrO)_{0.10}$	1.2×10^{-4}	1.4×10^{-3}	[228]
$(ThO_2)_{0.85}(SrO)_{0.15}$	1.3×10^{-4}	1.6×10^{-3}	[228]
$(ThO_2)_{0.90}(BaO)_{0.10}$	2.1×10^{-4}	3.0×10^{-3}	[228]
$(ThO_2)_{0.85}(BaO)_{0.15}$	4.3×10^{-4}	4.3×10^{-3}	[228]
$Th_{0.85}Y_{0.15}O_{1.925}$	1.8×10^{-3}	2.5×10^{-2}	[237]

significantly lower ionic conductivity than ceria, whereas the p-type conductivity of thoria in oxidizing conditions is higher. One can conclude, therefore, that the increasing atomic number of metal cations forming fluorite-type oxides leads to a decrease in anionic conduction and increasing electronic transport. For thoria, this general rule is illustrated using published data [237, 238, 242] which can be compared to the results on CeO_2-based solid solutions, considered above.

For applications in thermodynamic measurements, detailed investigations on electronic transport in $Th_{1-x}Me_xO_{2-\delta}$ (Me = Y and La, $x = 0.08$–0.20) solid electrolytes were performed [237–240, 242–245]. According to these results, the electrolytic domain where ThO_2-based ionic conductors can be used as solid electrolytes is displaced towards reducing oxygen pressures with respect to zirconia. Table 12 presents the reported regression parameters of the temperature dependence of the characteristic oxygen pressure P_e (atm), for some thoria-based solid solutions. P_e represents the oxygen partial pressure corresponding to equal ionic and n-type electronic conductivities, when

$$t_O = t_e = 0.5 \quad (5)$$

The temperature dependence of P_e can be approximated by

$$\log P_e = A - \frac{B}{T} \quad (6)$$

where A and B are regression parameters. Figure 8 shows the values of P_e determined by different authors.

Experimental data [237, 238, 244] show a clear enlargement of the electrolytic domain of the $Th(Y)O_{2-\delta}$ solid electrolytes with increasing yttria content, caused by both increasing ionic conductivity and displacement of the equilibrium concentrations of electronic species.

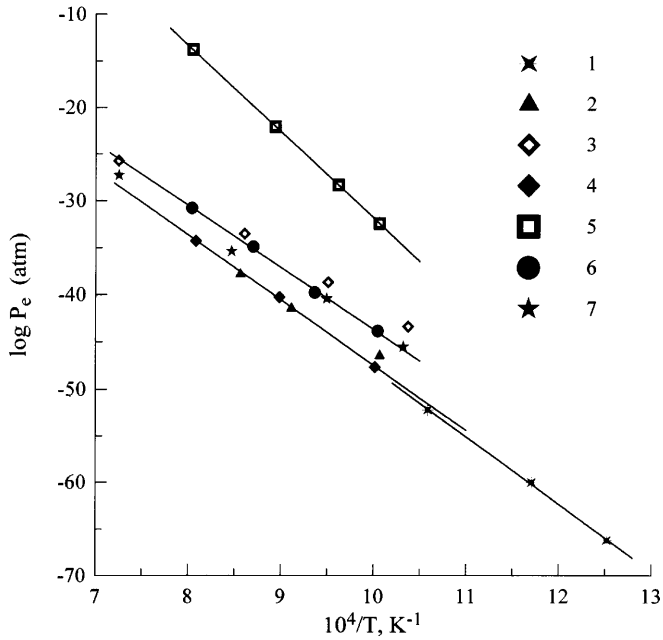

Fig. 8 Temperature dependence of the parameter P_e for the solid electrolytes $Th_{0.85}Y_{0.15}O_{1.925}$ (curves *1*, *2* [237] and *4* [242]) and $Th_{0.92}Y_{0.08}O_{1.96}$ (*curve 3*) [244]. Data [237] obtained using the cells W,Li,Li_2O|$Th(Y)O_{2-\delta}$|Fe,$Fe_{0.95}O$,Pt (*curve 1*) and W,Pb|$Th(Y)O_{2-\delta}$|Fe,$Fe_{0.95}O$,Pt (*curve 2*). *Curve 4* was calculated theoretically [242]. For comparison, similar results from refs. [273] (*curve 5*), [274] (*6*), and [275] (*7*) are also presented

Notice also that the P_e values from [242], calculated theoretically from the dissociation pressure of thorium dioxide, are close to experimentally measured values (Fig. 5). This shows that the ratio between the dissociation oxygen partial pressure and P_e should be approximately the same for fluorite-type oxides such as thoria and zirconia, and that electron mobility is also similar in the fluorites [239, 242].

Generally, results on ThO_2-based oxides demonstrate that such materials can be used in potentiometric cells to determine oxygen pressures at oxygen chemical potentials lower than those accessed with zirconia. However, the presence of significant p-type conductivity in oxidizing conditions prevents the use of air as a reference electrode [242]. Instead, various metal/metal oxide mixtures such as $Fe/FeO_{0.9}$ can be used. Examples of thoria solid electrolytes used for thermodynamic measurements have been published [6, 246, 247].

Table 12 Regression parameters of the temperature dependence of the oxygen partial pressure P_e for ThO_2-based solid electrolytes

Electrolyte	T (K)	$\log P_e$ (atm) $= A - B/T$		Ref.
		A	B	
$Th_{0.92}Y_{0.08}O_{1.96}$	1000–1400	13.36	56250	[244]
$Th_{0.85}Y_{0.15}O_{1.925}$	940–1140	10.71	57300	[237]
	800–940	21.46	70240	[237]
$Th_{0.85}Me_{0.15}O_{1.925}$ (Me = La, Y)	~1000	19.5	67000	[242, 243]

Electrochemical properties of ionic conductors based on HfO_2, CeO_2, and ThO_2

The specific properties of each group of oxides, considered above, determine their applicability in various electrochemical cells. The lower oxygen ionic conductivity of HfO_2- and ThO_2-based fluorite solid solutions with respect to stabilized zirconia limits possible applications of thoria and hafnia to devices operating at relatively high temperatures and reduced oxygen pressures (potentiometric sensors, thermodynamic measurements, protective coatings of electrochemical cells). As a result, the literature on electrochemical properties of hafnia- and thoria-based ionic conductors contains mainly the results of estimates for electrolytic domains [100, 158, 237, 239, 242–244], necessary for applications as measuring devices. In the framework of such studies, the theoretical aspects of oxygen permeation through fluorite-type ceramics were analyzed in detail (see [239, 248] and references herein), and a number of empirical methods to estimate the electrolytic domains was proposed [239]. In contrast to thoria- and hafnia- based solid electrolytes, ceria-containing oxides obtained more attention owing to their specific electrocatalytic properties, briefly considered below. Detailed analyses of the electrode processes in electrochemical cells with various oxide electrolytes were published in monographs [148, 158].

Electrochemical behavior of metal electrodes in contact with stabilized hafnia

Studies on the behavior of Pt and Ni electrodes in contact with $Hf(Y)O_2$ solid electrolytes [249, 250] were performed within research projects supervised by Perfilyev and Kuzin, and focused on fundamental aspects of electrochemical processes in cells with oxygen ion conductors (see [1, 148, 158] and references therein). The general comment is that the qualitative trends observed in the systems "metal/$Hf(Y)O_2$" [249, 250] are identical to those typical of electrochemical cells based on stabilized zirconia electrolytes [1, 148].

The cathodic polarization resistance of Ni electrodes in contact with hafnia stabilized with 12.5 mol% yttrium oxide increases with increasing hydrogen partial pressure in H_2/H_2O atmospheres [249], as found for nickel electrode layers applied onto $Zr(Y)O_2$ solid electrolyte substrates. Increasing water vapor pressure leads to increasing electrochemical activity and to a change in the shape of cathodic polarization curves. While the potential-current dependencies at high hydrogen pressures are Tafel-type, with high water vapor concentrations in the gas phase the polarization curves exhibit a tendency for limiting currents and a transition to Tafel behavior with further increase in current density. The potential for this transition is independent of the solid electrolyte material, having the same values for zirconia and hafnia electrolytes [148, 249]. Current treatment was found to lead to a significant change of the polarization resistance of nickel electrodes in contact with stabilized hafnia [249]. In particular, when the equilibrium potential of nickel electrodes is higher than the transition potential, treatment with anodic current results in increasing electrochemical activity, whereas the effect of cathodic current is the opposite. Possible mechanisms for such behavior were discussed in detail [148].

Comparative studies of platinum electrodes in contact with single crystals of $Hf(Y)O_2$ and $Zr(Y)O_2$ [250] also demonstrated qualitative resemblance for electrochemical processes involving these electrolytes. In particular, no influence of the crystallographic faces of the single crystals on electrode impedance was found. The dependence of impedance on the stabilizing dopant concentration showed maximum and minimum values along with a non-monotonous behavior, which was explained in terms of the interrelations between electronic conduction in the hafnia solid electrolytes and the electrode process mechanism [250].

Oxygen permeability of ceria-based mixed conductors

Oxygen permeation through La-doped cerium dioxide ceramics were found to increase with La_2O_3 content from 0 to 10 mol% [251], indicating an increase in both ionic and electronic conductivities of ceria. Therefore, increasing lanthanum concentration results in a change in the type of dominant electronic charge carriers from n-type, characteristic of undoped CeO_2, to electron holes. The p-type carriers form owing to incorporation of oxygen into vacancies created to balance the lanthanum additions [251]. Comparison of results on oxygen permeation [251] with data on n-type electronic conductivity [167] suggests a determining effect of trivalent dopant content on the electron band structure and, thus, on the chemical potential of oxygen ions in ceria. For applications of cerium oxide as a component of electrode materials, one can expect a better performance of REE-doped CeO_x having both higher ionic and electronic conductivities than the undoped oxide [251].

$Ce(Gd)O_{2-\delta}$ solid solutions doped with cobalt and manganese have been studied [181, 203, 252]. The solid solubility of Co and Mn in gadolinia-doped ceria (CGO) depends strongly on temperature, as found for the systems with stabilized zirconia doped with transition metals [1]. At temperatures of about 1270 K, the concentration limit for the fluorite solid solution formation corresponds to approximately 10 mol% for cobalt and 5 mol% for manganese. Quenching of the samples after annealing at higher temperature yields single-phase ceramics with a higher content of transition metal oxides [181, 203, 252]. Analogously to doped zirconia [1], incorporation of cobalt and manganese into the crystal lattice of CGO leads to decreasing ionic conductivity and increasing p-type electronic transport. Oxygen permeability at 1000–1300 K increases with increasing dopant concentration within the solid solution formation range, whereas segregation of cobalt and manganese oxide phases results in decreasing permeation fluxes and increasing total conductivity of the ceramics [181, 203, 252]. The permeation process through Co- and Mn-doped CGO is limited by conjugate bulk transport of oxygen ions and electron charge carriers. Deposition of porous platinum layers onto the membranes decreases the oxygen permeability owing to partial blocking at the surface.

Electrochemical properties of electrode systems with ceria-based electrolytes

A series of research articles by Perfilyev and Palguev [253–256] was focused on studying of platinum electrodes in contact with ceria solid electrolytes in air at temperatures of 923–1173 K. In the works [253, 254], dense platinum electrode layers were formed on the $0.85CeO_2$-$0.15CaO$ ceramics by annealing Pt powder at 1770–1800 K. Electrochemical properties of such electrodes were studied in the mode of pulse DC polarization as well as reversing the current. Analysis of the processes, observed at jump changes of the current density through the cell, allowed them to make a conclusion regarding the concentration nature of the polarization processes in these systems [253, 254]. The limiting stages of the anodic electrochemical reaction were determined to be oxygen diffusion through the solid electrolyte and through the electrode [253, 254]. Therewith, the diffusion fluxes through the electrode are significantly less than the fluxes through electrolyte. Increasing current density up to 1 A/cm^2 leads to decreasing polarization resistance of the dense electrodes, caused by distension of the anode interface layer of ceria electrolyte owing to evolution of molecular oxygen in pores of ceria, thus increasing the electrochemically active area. At higher current densities the anode layers were observed to exfoliate, which results in increasing polarization. Cathodic polarization resistance of the electrodes decreases moderately with increasing current density owing to partial reduction of the electrolyte surface layers with subsequent mechanical decomposition of ceria ceramics. As a general feature, electrochemical behavior of dense platinum electrodes was found to depend strongly on the pre-history of the cell [253, 254].

Detailed studies of porous platinum electrodes in contact with $Ce_{0.85}Ca_{0.15}O_{1.85}$ and $Zr_{0.85}Ca_{0.15}O_{1.85}$ electrolytes [255] indicated a chemical interaction of platinum with oxygen under the conditions of anodic polarization. No considerable differences in the electrochemical behavior of porous Pt electrodes applied on ceria- and zirconia-based electrolytes was found.

Polarization curves of platinum electrodes, deposited on the solid electrolyte ceramics $0.85CeO_2$-$0.15CaO$, $0.85CeO_2$-$0.15SrO$, and $0.85CeO_2$-$0.15La_2O_3$, can be described by a Tafel equation when the overpotential is higher than 50 mV [256]. For the anodic processes, there was observed an Arrhenius-type dependence of the exchange currents (i_0) on temperature:

$$i_0 = B \exp\left(-\frac{E_a}{RT}\right) \tag{7}$$

where B and E_a are the pre-exponential factor and activation energy, respectively. This suggests a single limiting stage for the electrochemical reaction. The activation energy calculated using Eq. 7 was 41, 32, and 15 kcal/mol for the electrolytes $0.85CeO_2$-$0.15CaO$, $0.85CeO_2$-$0.15SrO$, and $0.85CeO_2$-$0.15La_2O_3$, respectively. These values were noted to correlate with the activation energy for the ionic conductivity of the ceria-based solid solutions [256].

The results of impedance spectroscopy of the electrochemical cell

$$O_2(\mathrm{air}), Pt|0.85CeO_2\text{-}0.15CaO|Pt, O_2(\mathrm{air}) \tag{8}$$

at 973–1073 K did not allow unambiguous separation of the limiting stage of the reaction, but indicated that the limiting stage is probably not electrochemical [257]. The capacity of the electrical double layer was in the range 6.8–8.8 μF/cm^2 at zero polarization. Anodic polarization leads to a sharp increase in the capacity, which was as high as 9200 μF/cm^2 at 1073 K and 170 mV; the effect of cathodic polarization on the capacity was insignificant [257].

Testing the single SOFC-type cell

$$O_2(\mathrm{air}), Pt|0.85CeO_2\text{-}0.15CaO|Pt, CO \tag{9}$$

at 1273 K showed that the anodic polarization curves exhibit limiting currents [258]. Comparison of these experimental data and theoretical models proposed by Chebotin et al. [258] suggests that the limiting stage in this case refers to the reaction

$$O^{2-} + CO \rightarrow CO_2 + e^- \tag{10}$$

which takes place at the solid electrolyte surface. This reaction is promoted by electronic conductivity characteristic of ceria in reducing atmospheres. One should note the relatively high current densities (up to 1 A/cm^2) obtained using the cell (9), in spite of electronic conduction in the electrolyte.

On the basis of the results on the cells with ceria-based electrolytes (in particular, [258]), the conception of enlargement of the electrochemical reaction zone using mixed-conductive electrodes was formulated [148, 158]. At a later time, ceria was used as an activating addition to the anode layers.

Electrochemical activity of ceria-containing electrodes

Numerous experimental results [148, 259–265] show that incorporation of cerium oxides into metal and cermet electrodes, operating in reducing atmospheres under cathodic or anodic regimes, results in a great increase of the electrode layer's electrochemical activity. For example, incorporation of ceria into cermet electrodes consisting of a mixture of Pt and $Zr_{0.91}Sc_{0.09}O_{1.955}$ electrolyte leads to 4–5 times lower polarization resistance in the case of a H_2/H_2O atmosphere, and 3–4 times lower for CO/CO_2 mixtures [262]. For copper-based cermet electrodes, the drop in polarization resistance after addition of ceria was observed to be as high as 1000 times [259]. Introduction of ceria into the electrode material changes also the electrochemical reaction mechanism. Before activation with ceria the polarization curves for cermet cathodes comprising metals such as Pt, Pd, Ag, Ni, or Cu can be described by the Tafel equation. The activation results in linear overpotential-current dependencies up to overpotentials of 200–300 mV [259].

This important effect of cerium oxide additions may not be explained only by the mixed conductivity of $CeO_{2-\delta}$, as in [148]. For instance, the most significant reduction of the electrode polarization resistance can be achieved when ceria particles are uniformly distributed both on the surface and in the volume of the electrode porous matrix [148, 259, 263–265]. Such a distribution can be obtained after firing the metal or cermet electrode layer, in particular by impregnation with a solution of cerium salts such as nitrate or chloride, with subsequent annealing [264]. The $CeO_{2-\delta}$ powders prepared by thermal decomposition of cerium hydroxide or chloride, without additional thermal treatment, show maximum oxygen surface exchange rates with both molecular oxygen and CO_2, at temperatures above 570 K [266, 267]. Further thermal treatments, irrespective of the atmosphere, lead to passivation and decreasing surface exchange [266, 267]. Analogously, impregnation of SOFC anode cermets (already containing cerium dioxide before activation) with a solution of cerium nitrate was shown to result in a significant increase in the SOFC performance [264]. Therefore, the activating effect is caused by the specific electrocatalytic properties of highly dispersed ceria particles distributed on the electrode surface which participate in the electrochemical reaction and provide a high surface exchange rate. A similar role in the electrochemical process under oxidizing conditions may be played by PrO_x [148, 265, 268–272]. Practical recommendations, which follow from data on oxygen exchange, are considered below.

Oxygen exchange between cerium oxide and the gas phase

The results of oxygen exchange (OE) between ceria and the gas phase were reported by Kurumchin et al. [266, 267, 276–278], Sazonov et al. [176, 177], and Bakumenko et al. [174]. Comparative studies of oxygen desorption and oxygen exchange of rare-earth oxides [174, 176, 177, 279–282] showed that the properties of surface oxygen in $CeO_{2-\delta}$, with a composition close to stoichiometry are close to those found for other oxides such as La_2O_3 and Nd_2O_3. Significantly different behavior of the surface oxygen was observed for the praseodymium and terbium oxides, exhibiting a series of nonstoichiometric phases under the same conditions [174, 282]. CeO_x also forms such a series of phases [173] but at lower oxygen pressures. Hence, one can expect an increase in the surface exchange rate of cerium oxide at reduced concentrations of oxygen in the gas phase, when highly oxygen-deficient CeO_x phases are formed. This is confirmed by the appearance of an extremely high but unstable activity of cerium oxide powder quenched after annealing in vacuum at 970 K [176]. On the other hand, surface exchange properties of cerium oxide depend strongly on the history of samples [266, 267]. Maximum activity and minimum activation energy for the OE process are typical of freshly prepared powders starting from cerium metal salts (Table 13, Fig. 9). Prolonged annealing in either reducing or oxidizing conditions leads to passivation and decrease in the surface exchange rates. Therefore, the effect of annealing atmosphere on OE limiting stages is relatively small: after treatment in

Table 13 Effect of history on the parameters[a] of isotopic oxygen exchange between $CeO_{2-\delta}$ and gas phase [266]

Impurity content	Preparation method[b]	Treatment	E_R (kJ/mol)	n	R [mol/(s cm^2)] 800 K	R [mol/(s cm^2)] 870 K
<0.1%	DH	As-prepared	63 ± 2	0.2	7.9×10^{-11}	1.5×10^{-10}
<0.1%		vacuum, 1233 K, 4 h	158 ± 6	–	–	9.0×10^{-12}
<0.1%		$CO + CO_2$ (12 vol% CO), 1173 K, 337 h	175 ± 5	–	6.9×10^{-12}	5.3×10^{-11}
<0.1%		$CO + CO_2$, 1173 K, 337 h and then vacuum, 1233 K, 4 h	167 ± 6	0.6	–	5.9×10^{-11}
<0.1%	DC	as-prepared	135 ± 5	0.2	2.9×10^{-11}	–
<0.1%		vacuum, 1233 K, 4 h	183 ± 6	–	3.1×10^{-12}	–
<0.1%		H_2+H_2O (90% H_2), 1173 K, 400 h	188 ± 6	0.1	–	8.0×10^{-11}
<0.1%		H_2+H_2O (90% H_2), 1173 K, 400 h; and then vacuum, 1233 K, 4 h	167 ± 5	0.1	8.1×10^{-12}	5.4×10^{-11}
<0.1%		H_2+H_2O (10% H_2), 1173 K, 400 h	188 ± 6	0.4	6.3×10^{-12}	4.8×10^{-11}
<0.1%		H_2+H_2O (10% H_2), 1173 K, 400 h; and then vacuum, 1233 K, 4 h	175 ± 5	–	–	3.0×10^{-11}
<0.005%	S	vacuum, 1233 K, 4 h	189 ± 6	–	9.0×10^{-13}	8.3×10^{-12}

[a] R is the rate of oxygen isotopic heteroexchange; E_R is the activation energy for the exchange rate; n is the exchange reaction order

[b] DH and DC correspond to thermal decomposition of cerium hydroxide and cerium chloride at 1123 K in air, respectively. S means sintering in air at 1373 K for 4 h

vacuum, hydrogen, carbon monoxide, and atmospheric air, CeO_x powders exhibit similar values of activation energy for the oxygen hetero-exchange, which varies from 158 to 188 kJ/mol [266]. Analogously to stabilized zirconia and rare-earth metal oxides, the OE reaction between CeO_x and the gas phase involves predominantly two oxygen atoms of the oxide lattice surface layer (so-called exchange type III) [174, 177, 266], but the contribution of the OE type II, with one participating atom from the lattice, is also significant [266].

The OE rate between CeO_x and the gas phase containing molecular oxygen increases regularly with increasing oxygen pressure (Fig. 10). The OE reaction order was reported to vary from 0.1 to 1.0 [176, 266], indicating a complex mechanism for the OE reaction. In particular, the reaction order values close to 0.2, which are typical for $CeO_{2-\delta}$ powders prepared in air (Table 13), permit assumption of the participation of fluorite lattice defects such as electron holes and oxygen vacancies in the exchange process.

Testing heterophase oxygen exchange between CeO_x and CO_2 [267] demonstrated significantly higher exchange rates and lower activation energies with respect to the OE reaction between cerium oxide and molecular oxygen (Fig. 9). This may be associated with formation of carbonate ions (CO_3^{2-}) at the oxide surface, at some intermediate stage of the OE reaction [267, 276].

When discussing the OE process under moderate oxygen chemical potentials [266, 267, 276–278], one should note the great effect of the oxygen vacancy concentration and electronic conduction on the electrocatalytic activity of cerium oxide. First of all, increasing impurity or dopant content leads to higher OE rates due to probably higher concentrations of oxygen vacancies and electronic conductivity, as discussed above. From the viewpoint of influence of the electronic conduction on oxygen exchange, doped ceria exhibits an intermediate behavior between stabilized zirconia and stabilized bismuth oxide [276–278]. In the case of zirconia, the OE reaction is limited by the electronic transport at the electrolyte surface and increases with deposition of electron-conducting layers onto the surface. For stabilized Bi_2O_3, the OE process is delocalized at the electrolyte surface, and electrodes play mainly the role of current collectors. For La-doped $Ce(Gd)O_{2-\delta}$, the oxygen exchange rates are close to those of bismuth oxide electrolytes. However, the exchange process between the gas phase and the ceria solid electrolyte with deposited Pt layers was found to occur on both metal and oxide surfaces [276, 277]. As a result, deposition of porous platinum onto ceria surface may increase OE currents.

The analysis of experimental data on oxygen exchange [176, 177, 266, 267, 276–278] suggests the following conclusions:

1. A maximum effect of cerium oxide additions on the performance of electrodes operating in reducing conditions can be expected in the case of low operating temperatures, when the rate of passivation of ceria electrocatalysts is moderate. However, low operating temperatures also limit the reversibility of

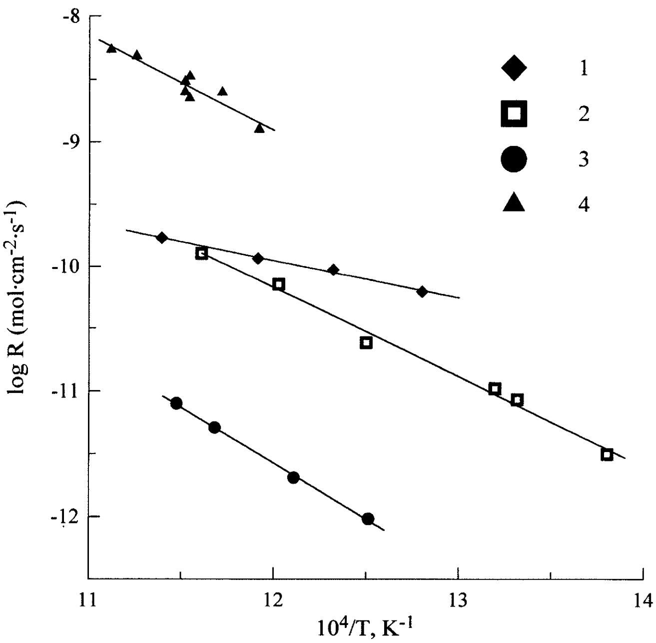

Fig. 9 Temperature dependence of the $CeO_{2-\delta}$ oxygen isotopic exchange rate: *1* as-prepared powder obtained by thermal decomposition of cerium hydroxide at 1123 K in air; *2*, as-prepared powder obtained by thermal decomposition of cerium chloride in air; *3*, oxide powder annealed at 1373 K for 4 h in air; *4* ceramics sintered in air at 2100 K. *Curves 1–3* correspond to exchange with molecular oxygen [266]. *Curve 4* presents data on oxygen exchange with carbon dioxide [267]

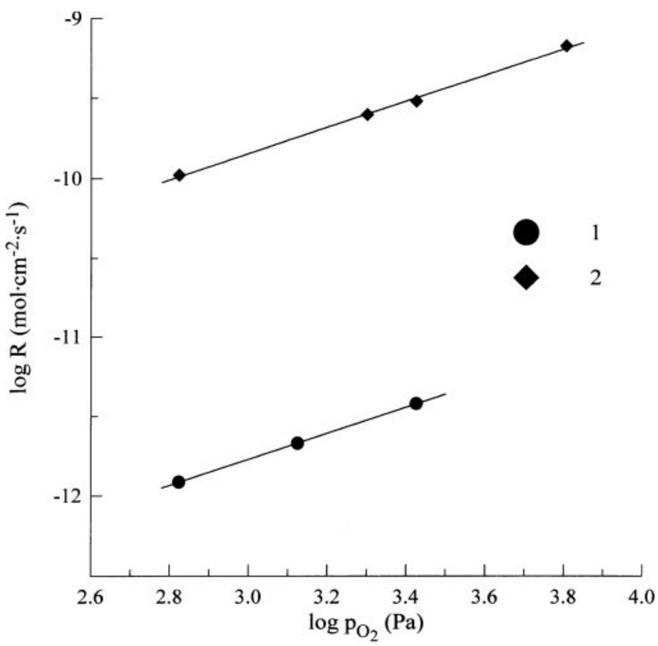

Fig. 10 Oxygen partial pressure dependence of *1* oxygen isotopic exchange rate at 688 K and *2* oxygen homomolecular exchange rate at 763 K on $CeO_{2-\delta}$ [176]

electrodes, as well as oxygen substoichiometry and electronic conduction in cerium oxide. An optimum working temperature might be compatible for electrochemical cells with solid electrolytes based on $LaGaO_3$ and $Ce(Gd)O_{2-\delta}$.
2. As the surface of doped ceria ionic conductors plays an important role in the OE process, an increase in the exchange currents and hence a decrease in polarization resistance of the electrode systems can be achieved by increasing the specific surface area of the $Ce(Me)O_{2-\delta}$ solid electrolyte ceramics.
3. Since the electrocatalytic activity of cerium oxide increases with reducing conditions and increasing electronic conduction, which is not acceptable for solid electrolytes, a positive effect can be obtained using multi-layer cells where the composition of the outer anode layer is designed from a viewpoint of optimized catalytic properties.

Electrochemical properties of perovskite-type cerates

Other promising ion-conducting materials are the $MCeO_{3-\delta}$ perovskite-type cerates which possess a mixed oxygen ionic and p-type electronic conduction at high oxygen pressures, but have predominant protonic conductivity in hydrogen-containing atmospheres [200, 201, 283, 284]. Partial substitution of cerium cations with trivalent rare-earth ions leads to increasing oxygen ion vacancy concentration and, therefore, ionic conduction. The optimum dopant concentration in $MCe_{1-x}Me_xO_{3-\delta}$ varies in the range of x from 0.06 to 0.15 [200, 201]. In the case of strontium cerate, the maximum protonic conduction is observed when incorporating Gd, Dy, or Yb into the cerium sublattice [200], whereas the best ionic transport properties of $BaCeO_{3-\delta}$-based ceramics can be achieved using Nd, Eu, Gd, Dy, Ho, or Lu [201]. Testing of single SOFCs with a $BaCe_{0.90}Nd_{0.10}O_{3-\delta}$ solid electrolyte, one Ni cermet, and $La_{0.8}Sr_{0.2}MnO_{3-\delta}$ electrodes demonstrated sufficient cell stability [283]. A high electrochemical activity of the cermet and manganite electrode layers in contact with doped barium cerate was ascertained from detailed investigations of their polarization characteristics [283]. At the same time, the proton-conducting cerates exhibit specific thermal expansion features, hampering their practical use [284]. In particular, anomalies in thermal expansion of the $BaCe_{1-x}Me_xO_{3-\delta}$ (Me = Er, Nd) solid solutions, associated with change in the atmospheric humidity and history of the electrolytes, were found while testing the materials in atmospheres with variable water vapor concentration [284].

Final remarks

While the driving force for this review was the dissemination of information published in the former Soviet Union, on high-temperature oxygen electrochemistry, the obvious conclusion of this work is that new materials with improved properties, for high technology applications of solid electrolytes, were studied for many years in all advanced research centers, irrespective of well-known constraints. Knowledge and technological development had to face the same challenges everywhere. If dissemination of information could be limited by specific constraints including language problems, outstanding contributions to the field were always recognized worldwide. This explains to a reasonable extent the already mentioned coherence but also parallelism between research results now presented and those more familiar to readers of scientific journals commonly edited in English. Most pioneering contributions quickly spread and became part of common knowledge.

In fact, in 1970, Etsell and Flengas [285] already wrote a rather complete review on oxygen ionic conductors, covering almost 700 references, with an enormous variety of data sources and authors. This is still an invaluable reference to newcomers. The present contribution, besides other objectives already presented, can be understood also as an attempt to complement and update this pioneering work. New ideas and materials were developed in the last 30 years, and experimental techniques provide nowadays a deeper knowledge and understanding of relevant phenomena in the field.

References

1. Kharton VV, Naumovich EN, Vecher AA (1999) J Solid State Electrochem 3: 61
2. Glushkova VB, Kravchinskaya MV, Kusnetsov AK, Tikhonov PA (1984) Hafnium dioxide and its compounds with rare-earth element oxides. Nauka, Leningrad (in Russian)
3. Bogdanov AG, Rudenko VS, Makarov LP (1965) Dokl Akad Nauk SSSR 160: 1065
4. Bendeliani NA, Popova SV, Vereschagin LF (1967) Geokhimiya: 677
5. Kornilov II, Glazova VV, Ruda GI (1968) Neorg Mater 4: 2106
6. Vasilyeva IA, Granovskaya ZhV (1980) Zh Fiz Khim 54: 1009
7. Marushkin KN, Alikhanyan AS, Orlovskiy VP (1990) Zh Neorg Khim 35: 2071
8. Chebotin VN, Volchenkova ZS, Palguev SF (1964) Trudy Inst Elektrokhim 5: 123
9. Zubankova DS, Volchenkova ZS (1976) Trudy Inst Elektrokhim 23: 89
10. Redko VP, Terekhovskiy PB, Mayster IM, Shevchenko AV, Lopato LM, Dvernyakova AA (1990) Neorg Mater 26: 1247
11. Gavrish AM, Sukharevsky BYa, Zoz EI, Solov'eva AE (1971) Dokl Akad Nauk SSSR 199: 880
12. Filatov SK, Frank-Kamenetsky VA (1969) Kristallografiya 14: 804
13. Berezhnoy AS, Belik VYa, Gavrish AM, Gulko NV (1968) Neorg Mater 4: 1605
14. Portnoy KI, Timofeeva NI, Salibekov SE, Romanovich IV (1970) Neorg Mater 6: 91
15. Korsakov IE (1993) PhD Thesis. Moscow State University, Moscow
16. Zoz EI, Lopato LM, Gulko NV (1983) Neorg Mater 19: 1702
17. Redko VP (1990) PhD Thesis. Institute of Material Science Problems, Ukrainian Academy of Sciences, Kiev

18. Gavrish AM, Sukharevsky BYa, Zoz EI (1975) Dokl Akad Nauk SSSR 222: 1343
19. Volchenkova ZS, Palguev SF (1964) Trudy Inst Elektrokhim 5: 133
20. Strekalovsky VN, Burov GV, Samarina VA, Volchenkova ZS (1964) Trudy Inst Elektrokhim 5: 163
21. Shevchenko AV, Lopato LM, Gerasimyuk GI, Zaitseva ZA (1981) Neorg Mater 17: 838
22. Lopato LM, Shevchenko AV, Zoz EI, Gerasimyuk GI (1981) Neorg Mater 17: 90
23. Kuznetsov AK, Tikhonov PA, Kravchinskaya MV (1975) Zh Neorg Khim 20: 758
24. Godina NA, Keler EK (1959) Zh Neorg Khim 4: 884
25. Andrievskaya ER (1989) PhD Thesis. Institute of Material Science Problems, Ukrainian Academy of Sciences, Kiev
26. Lopato LM, Andrievskaya ER, Shevchenko AV (1988) Neorg Mater 24: 1861
27. Keler EK, Godina NA, Degen MG (1961) Zh Prikl Khim 34: 1769
28. Andrievskaya ER, Shevchenko AV, Lopato LM, Zaytseva ZA (1989) Neorg Mater 25: 1576
29. Gavrish AM, Sukharevsky BYa, Zoz EI, Solov'eva AE (1973) Neorg Mater 9: 260
30. Shevchenko AV, Lopato LM, Gerasimyuk GI, Zaitseva ZA (1987) Neorg Mater 23: 1495
31. Danilenko VM, Lopato LM, Andrievskaya ER (1991) Neorg Mater 27: 1859
32. Andrievskaya ER, Lopato LM (1991) Neorg Mater 27: 1863
33. Lopato LM, Andrievskaya ER, Zaitseva ZA, Shevchenko AV (1991) Neorg Mater 27: 1866
34. Andrievskaya ER, Kovylyaev VV, Lopato LM (1991) Neorg Mater 27: 1871
35. Karpenko YuM, Lopato LM, Gerasimyuk GI, Shevchenko AV (1991) Neorg Mater 27: 2341
36. Shevchenko AV, Lopato LM, Karpenko YuM, Gerasimyuk GI (1991) Neorg Mater 27: 2444
37. Leont'ev NG, Kolesova RV, Eremkin VV, Smotrakov VG, Fesenko OE (1984) Neorg Mater 20: 2009
38. Andrievskaya ER, Lopato LM, Kiryakova IE (1993) Neorg Mater 29: 530
39. Andrievskaya ER, Kiryakova IE, Lopato LM (1991) Neorg Mater 27: 2161
40. Reznitsky LA (1985) Neorg Mater 21: 1801
41. Narchuk PB, Kovba ML, Levitsky VA (1981) Dokl Akad Nauk SSSR 256: 117
42. Vishnevsky II, Skripak VN (1970) Ogneupory (11): 16
43. Sorokina SL, Skolis YuYa, Levitsky VA (1986) Zh Fiz Khim 60: 265
44. Reznitsky LA (1985) Zh Fiz Khim 59: 815
45. Gvelesiani GG, Padiradze AA, Omiadze IS, Levitsky VA, Narchuk PB (1983) Teplofiz Vys Temp 21: 1023
46. Levitsky VA, Narchuk PB, Kashkarova SL (1982) Zh Fiz Khim 56: 803
47. Redko VP, Shevchenko AV, Lopato LM (1988) Neorg Mater 24: 2027
48. Shevchenko AV, Zaytseva ZA, Lopato LM, Gerasimyuk GI (1983) Neorg Mater 19: 2059
49. Belik VYa (1967) Dokl Akad Nauk USSR Ser B 618
50. Berezhnoy AS, Belik VYa (1967) Dokl Akad Nauk USSR Ser B 708
51. Scherbakova LG, Glushkova VB, Sapozhnikov RA (1977) Neorg Mater 13: 674
52. Tikhonov PA, Kuznetsov AK, Krasilnikov MD, Kravchinskaya MV (1977) Zh Fiz Khim 51: 143
53. Volchenkova ZS, Zubankova DS (1982) Neorg Mater 18: 2009
54. Kravchinskaya MV, Tikhonov PA, Kuznetsov AK (1978) Neorg Mater 14: 1314
55. Zubankova DS, Volchenkova ZS (1979) Trudy Inst Elektrokhim 28: 107
56. Shevchenko AV, Lopato LM (1982) Neorg Mater 18: 1842
57. Teterin GA, Semenov GA, Shkolnikova TM, Menchuk EM, Kulinina LA, Semin EG, Borisova VB (1989) Neorg Mater 25: 1574
58. Komissarova LN, Spiridonov FM (1968) Dokl Akad Nauk SSSR 182: 834
59. Shevchenko AV, Mayster IM, Lopato LM (1987) Neorg Mater 23: 1320
60. Zyrin AV, Redko VP, Lopato LM, Shevchenko AV, Mayster IM, Zaytseva ZA (1987) Neorg Mater 23: 1325
61. Volchenkova ZS, Zubankova DS (1975) Trudy Inst Elektrokhim 22: 107
62. Redko VP, Lopato LM (1992) Neorg Mater 28: 1902
63. Lopato LM, Redko VP, Gerasimyuk GI, Shevchenko AV (1990) Poroshk Metall (4): 73
64. Shevchenko AV, Lopato LM, Kiryakova IE (1984) Neorg Mater 20: 1991
65. Volchenkova ZS, Zubankova DS, Gorelov VP (1976) Trudy Inst Elektrokhim 24: 66
66. Volchenkova ZS, Zubankova DS (1976) Trudy Inst Elektrokhim 23: 83
67. Glushkova VB, Markov NI, Osiko VV, Tatarintsev VM, Tikhonov PA (1983) Neorg Mater 19: 1689
68. Portnoy KI, Romanovich IV, Timofeeva IN (1971) Neorg Mater 7: 888
69. Isupova EN, Glushkova VB, Keler EK (1969) Neorg Mater 5: 1948
70. Marushkin KN (1996) Neorg Mater 32: 342
71. Voronko YuK, Sobol AA, Tsimbal LI (1998) Neorg Mater 34: 1306
72. Sukharevsky BYa, Gavrish AM, Zoz EI, Solov'eva AE (1973) Dokl Akad Nauk SSSR 208: 1086
73. Marushkin KN, Alikhanyan AS (1991) Zh Neorg Khim 36: 2637
74. Popov SG, Paromova MV, Kulikova ZYa, Rozanova ON, Pashin SF (1990) Neorg Mater 26: 1002
75. Voronko YuK, Sobol AA, Tsimbal LI (1998) Neorg Mater 34: 439
76. Spiridonov FM, Komissarova LN, Kocharov AG, Spitsyn VI (1969) Zh Neorg Khim 14: 2535
77. Vlasov AN, Savitsky AA (1989) Elektrokhimiya 25: 1394
78. Zubankova DS, Volchenkova ZS (1976) Trudy Inst Elektrokhim 23: 89
79. Zhidovinova SV, Kotlyar AG, Strekalovskiy VN, Palguev SF (1972) Trudy Inst Elektrokhim 18: 148
80. Zhidovinova SV (1974) PhD Thesis. Institute of Electrochemistry, Ural Dept. of Academy of Sciences of USSR, Sverdlovsk
81. Shevchenko AV, Lopato LM, Zaytseva ZA (1984) Neorg Mater 20: 1530
82. Komissarova LN, Van Gan-Shi, Spitsyn VI, Simanov YuP (1964) Zh Neorg Khim 9: 693
83. Fomina LN, Palguev SF (1978) Trudy Inst Elektrokhim 27: 93
84. Volchenkova ZS, Zubankova DS (1982) Neorg Mater 18: 2009
85. Zhidovinova SV, Strekalovskiy VN, Palguev SF (1972) Comparative character of phase formation at interaction of yttrium and rare-earth elements oxides with zirconium and hafnium oxides. VINITI, Sverdlovsk (in Russian)
86. Shevchenko AV, Lopato LM (1975) Dokl Akad Nauk USSR Ser B 735
87. Sukharevsky BYa, Zoz EI, Gavrish AM, Gulko NV (1977) Dokl Akad Nauk SSSR 237: 589
88. Shevchenko AV, Lopato LM, Ruban AK (1976) Dokl Akad Nauk USSR Ser B 922
89. Spiridonov FM, Chiong L, Komissarova LN (1977) Zh Neorg Khim 22: 588
90. Gavrish AM, Zoz EI, Gulko NV, Solovyeva AE (1975) Neorg Mater 11: 668
91. Shevchenko AV, Mayster IM, Lopato LM, Zaytseva ZA (1983) Neorg Mater 19: 843
92. Kulikov VD, Melnikov AV, Zaslavsky AN (1989) Zh Neorg Khim 34: 2707

93. Kravchinskaya MV, Tikhonov PA, Kuznetsov AK (1978) Neorg Mater 14: 1314
94. Kuznetsov AK, Tikhonov PA, Kravchinskaya MV (1976) Zh Neorg Khim 21: 1317
95. Kravchinskaya MV, Tikhonov PA, Kuznetsov AK, Ganits F (1978) Dokl Akad Nauk SSSR 238: 583
96. Zhidovinova SV, Kotlyar AG, Strekalovsky VN, Palguev SF (1972) Trudy Inst Elektrokhim 18: 148
97. Shevchenko AV, Lopato LM (1977) Dokl Akad Nauk USSR Ser B 718
98. Tikhonov PA, Sazonova LV, Glushkova VB, Kravchinskaya MV (1980) Zh Fiz Khim 54: 1967
99. Glushkova VB, Sazonova LV, Ganits F (1978) Neorg Mater 14: 2096
100. Zubankova DS, Volchenkova ZS (1979) Trudy Inst Elektrokhim 28: 107
101. Shevchenko AV, Lopato LM, Nazarenko LV (1984) Neorg Mater 20: 1862
102. Isupova EN, Glushkova VB, Keler EK(1968) Neorg Mater 4: 399
103. Zhidovinova SV, Strekalovskiy VN, Palguev SF (1975) Neorg Mater 11: 1809
104. Andrievskaya ER, Lopato LM, Shevchenko AV, Smirnov VP (1997) Neorg Mater 33: 835
105. Shevchenko AV, Lopato LM, Stegniy AI, Mayster IM, Dvernyakov VS, Pasichniy VV (1979) Dokl Akad Nauk USSR Ser A 585
106. Volchenkova ZS, Zubankova DS (1987) Neorg Mater 23: 1175
107. Isupova EN, Glushkova VB, Keler EK (1968) Neorg Mater 4: 1732
108. Spiridonov FM, Komissarova LN (1970) Zh Neorg Khim 15: 875
109. Redko VP, Lopato LM (1992) Neorg Mater 28: 1902
110. Perova EB, Samoylenko AA, Spiridonov FM, Komissarova LN (1972) Zh Neorg Khim 17: 2846
111. Shevchenko AV, Lopato LM, Tkachenko VD, Ruban AK (1987) Neorg Mater 23: 259
112. Gavrish IM, Sukharevskiy BYa, Kriviruchko PP, Zoz EI (1969) Neorg Mater 5: 547
113. Fomina LN, Palguev SF (1978) Trudy Inst Elektrokhim 27: 93
114. Shevchenko AV, Lopato LM, Gerasimyuk GI, Tkachenko VD (1990) Neorg Mater 26: 839
115. Mayster IM, Shevchenko AV, Lopato LM, Redko VP, Ruban AK, Terekhovsky PB (1990) Neorg Mater 26: 1007
116. Shevchenko AV, Mayster IM, Lopato LM, Tkachenko VD (1989) Neorg Mater 25: 989
117. Shevchenko AV, Lopato LM, Obolonchik TV, Tkachenko VD, Nazarenko LV (1987) Neorg Mater 23: 452
118. Obolonchik TV, Lopato LM, Gerasimyuk GI, Shevchenko AV (1991) Neorg Mater 27: 2345
119. Andrievskaya ER, Lopato LM, Danilenko VM (1993) Neorg Mater 29: 535
120. Perova EB, Spiridonov FM, Komissarova LN (1972) Neorg Mater 8: 1878
121. Andrievskaya ER, Lopato LM, Kovylyaev VV, Zaytseva ZA (1996) Neorg Mater 32: 727
122. Komissarova LN, Spiridonov FM, Spitsyn VI (1968) Dokl Akad Nauk SSSR 181: 881
123. Vlasov AN, Palguev SF (1975) Dokl Akad Nauk SSSR 221: 364
124. Glushkova VB, Komarov AV, Markov NI, Osiko VV, Tatarintsev VM, Tikhonov PA (1986) Neorg Mater 22: 1131
125. Alekseenko LS, Sharova NM, Gulko NV, Gudilina AI (1975) Ogneupory (5): 36
126. Vlasov AN (1989) Elektrokhimiya 25: 1313
127. Gorelov VP, Palguev SF (1979) Dokl Akad Nauk SSSR 248: 1356
128. Volchenkova ZS (1969) Neorg Mater 5: 1096
129. Vlasov AN (1983) Elektrokhimiya 19: 1624
130. Perfilyev MV, Inozemtsev MV, Vlasov AN (1982) Elektrokhimiya 18: 1230
131. Paputsky YuN, Krzhizhanovskaya VA, Glushkova VB (1974) Neorg Mater 10: 1551
132. Koryakina EL, Zoz EI, Gavrish AM, Gulko NV (1978) Zh Neorg Khim 23: 3202
133. Lopato LM, Redko VP, Veblaya TS, Kharchenko NP (1992) Neorg Mater 28: 2250
134. Krzhizhanovskaya VA, Scherbakova LG, Keler EK, Glushkova VB (1972) Neorg Mater 8: 536
135. Glushkova VB, Grischenko VI, Krzhizhanovskaya VA, Keler EK (1976) Neorg Mater 12: 695
136. Glushkova VB, Krzhizhanovskaya VA, Dyakovsky VS, Abramova VM (1975) Neorg Mater 11: 964
137. Kolesnikov AV, Scherbakova LG, Breusov ON (1981) Dokl Akad Nauk SSSR 256: 113
138. Karaulov AG, Rudyak IN, Taranukha HM, Glushko LI (1974) Neorg Mater 10: 1281
139. Glazachev VS, Lukin ES, Balashov VA, Borovkina (1976) Mechanism of formation of the solid solutions in Y_2O_3-HfO_2 and Y_2O_3-ZrO_2 systems. VINITI, Moscow (in Russian)
140. Glazachev VS, Lukin ES, Balashev VA, Borovkova LB (1977) Neorg Mater 13: 1814
141. Sukharev YuG, Akulyushin IL, Mironov VS, Andriyanov AV, Zherevchuk VV (1994) Neorg Mater 30: 556
142. Sukharev YuG, Akulushin IL, Zherevchuk VV, Savelyev AA, Andriyanov AV, Mironov VS, Polyarush OV (1997) Neorg Mater 33: 1478
143. Shevchenko AV, Lopato LM, Mayster IM, Zaytseva ZA (1980) Neorg Mater 16: 1980
144. Shevchenko AV, Mayster IM, Lopato LM (1977) Dokl Akad Nauk USSR Ser A 279
145. Lopato LM, Shevchenko AV, Gerasimyuk GI (1976) Neorg Mater 12: 1623
146. Spiridonov FM, Mulenkova MN, Tsirelnikov VI, Komissarova LN (1981) Zh Neorg Mater 26: 1705
147. Morozova LV, Tikhonov PA, Glushkova VB (1991) Neorg Mater 27: 291
148. Perfilyev MV, Demin AK, Kuzin BL, Lipilin AS (1988) High-temperature electrolysis of gases. Nauka, Moscow (in Russian)
149. Strekalovsky VN, Polezhaev YuM, Palguev SF (1987) Oxides with impurity-caused disorder. Composition, structure, phase transitions. Nauka, Moscow (in Russian)
150. Gorelov VP (1978) Trudy Inst Elektrokhim 26: 69
151. Gorelov VP, Palguev SF (1979) Dokl Akad Nauk SSSR 248: 1356
152. Vlasov AN (1989) Elektrokhimiya 25: 699
153. Poluyan AF (1987) PhD Thesis. Belarus State University, Minsk
154. Kudo T, Obayashi H (1976) J Electrochem Soc 123: 415
155. Hammou A (1975) J Phys Chem 72: 431
156. Palguev SF, Gilderman VK, Neujmin SF (1975) J Electrochem Soc 122: 745
157. Leonov AI (1970) High-temperature chemistry of cerium compounds with oxygen. Nauka, Leningrad (in Russian)
158. Chebotin VN, Perfilyev MV (1978) Electrochemistry of solid electrolytes. Khimiya, Moscow (in Russian)
159. Volchenkova ZS, Nedopekin VM, Sizintseva NF (1978) Trudy Inst Elektrokhim 26: 76
160. Poluboyarinov DN, Shapiro EYa, Bakunov VS, Akopov FA (1966) Neorg Mater 2: 336
161. Bogoroditsky IP, Pasynkov VV, Basili RR, Volokobinsky YuM (1965) Dokl Akad Nauk SSSR 160: 578
162. Vinokurov IV, Zonn ZN, Ioffe VA (1967) Neorg Mater 3: 1012
163. Volchenkova ZS, Gorelov VP (1978) Electrical conductivity of purified CeO_2. In: Ionic melts and solid electrolytes. Academy of Sciences of USSR, Sverdlovsk, pp 88–92 (in Russian)
164. Vinokurov IV, Zonn ZN, Ioffe VA (1967) Fiz Tverdogo Tela 9: 3369
165. Miloslavsky AG, Zhuravlev NL (1983) Fiz Tverd Tela 13: 58
166. Miloslavsky AG, Zhuravlev NL (1984) Fiz Tverd Tela 14: 23
167. Neuimin AD, Palguev SF, Chebotin VN (1963) Trudy Inst Elektrokhim 4: 97

168. Vinokurov IV (1970) Neorg Mater 6: 31
169. Kuznetsov FA, Rezukhina TN (1960) Zh Fiz Khim 34: 2467
170. Kuznetsov FA, Rezukhina TN, Golubenko AN (1960) Zh Fiz Khim 34: 2129
171. Kuznetsov FA, Rezukhina TN (1961) Zh Fiz Khim 35: 956
172. Kuznetsov FA, Belyi VI, Rezukhina TN, Gerasimov YaI (1961) Dokl Akad Nauk SSSR 139: 1405
173. Rudenko VS, Boganov AG (1971) Neorg Mater 7: 108
174. Bakumenko TT, Moroz NF (1974) Kinet Katal 15: 452
175. Lyando VA (1966) Kinet Katal 3: 475
176. Sazonov LA, Sokolovsky VD, Boreskov GK (1966) Kinet Katal 7: 521
177. Sazonov LA, Artamonov EV, Mitrofanova GN (1971) Kinet Katal 12: 378
178. Vinokurov IV, Zonn ZN, Ioffe VA (1965) Fiz Tverd Tela 7: 1012
179. Oliva C, Termignone G, Vatti FP, Forni L, Vishniakov AV (1996) J Mater Sci 31: 6333
180. Strekalovsky VN, Palguev SF (1970) XRD studies of solid solutions of oxides with fluorite structure. In: Rentgenografiya mineralnogo syr'ya, vol. 7. Nedra, Moscow, pp 30–46
181. Kovalevsky AV, Kharton VV, Naumovich EN (1996) Neorg Mater 32: 1401
182. Solov'eva AE, Gavrish AM, Zoz EI (1974) Neorg Mater 10: 469
183. Palguev SF, Volchenkova ZS (1961) Trudy Inst Elektrokhim 2: 157
184. Yushina LD, Palguev SF (1963) Trudy Inst Elektrokhim 4: 91
185. Neuymin AD, Palguev SF (1962) Trudy Inst Elektrokhim 3: 141
186. Strekalovsky VN, Burov GV, Samarina VA, Palguev SF, Volchenkova ZS (1962) Trudy Inst Elektrokhim 3: 171
187. Reznitsky LA (1986) Zh Fiz Khim 60: 987
188. Keler EK, Godina NA, Kalinina AM (1956) Zh Neorg Khim 1: 2556
189. Vovkotrub EG, Strekalovsky VN (1988) Zh Prikl Spectrosc 49: 50
190. Sorokina SL, Skolis YuYa, Kovba ML, Levitsky VA (1986) Zh Fiz Khim 60: 310
191. Strekalovsky VN, Burov GV, Palguev SF, Volchenkova ZS, Samarina VA (1962) Trudy Inst Elektrokhim 3: 165
192. Keler EK, Godina NA (1957) Zh Neorg Khim 2: 209
193. Levitsky VA, Sorokina SL, Skolis YuYa, Kovba ML (1985) Neorg Mater 21: 1357
194. Galakhov FYa (ed) (1987) Phase diagrams of high-melting oxide systems. A handbook, vol. 5. Nauka, Leningrad (in Russian)
195. Neuimin AD, Palguev SF (1961) Trudy Inst Elektrokhim 2: 185
196. Neuimin AD, Palguev SF (1962) Trudy Inst Elektrokhim 3: 133
197. Zhdanova GM, Neuimin AD, Palguev SF, Ovchinnikov YuM (1966) Trudy Inst Elektrokhim 9: 167
198. Palguev SF, Yushina LD, Ovchinnikov YuM (1961) Trudy Inst Elektrokhim 2: 193
199. Gorelov VP (1988) Elektrokhimiya 24: 1380
200. Gorelov VP, Zubankova DS (1992) Elektrokhimiya 28: 944
201. Gorelov VP, Sharova NV, Sokolova YuV (1997) Elektrokhimiya 33: 1455
202. Palguev SF, Karpachev SV, Neuimin AD, Volchenkova ZS (1960) Dokl Akad Nauk SSSR 134: 1138
203. Naumovich EN, Kharton VV, Kovalevsky AV, Samokhval VV (1998) Fluorite-like mixed conductors in the systems $Bi(Y,M)O_{1.5\pm\delta}$ (M = Pr,Co) and $Ce(Gd,Me)O_{2-\delta}$ (Me = Co, Mn). In: Ramanarayanan TA (ed) Ionic and mixed conducting ceramics III. The Electrochemical Society, Pennington, NJ, pp 496–508
204. Palguev SF, Volchenkova ZS (1960) Zh Fiz Khim 34: 452
205. Palguev SF, Alyamovskiy SI, Volchenkova ZS (1959) Zh Neorg Khim 4: 2571
206. Volchenkova ZS, Palguev SF (1967) Trudy Inst Elektrokhim 10: 119
207. Toropov NA, Barzakovskii VP, Lapin VV, Kurtseva NN (1965) Phase diagrams of silicate systems. A handbook, vol. 1. Nauka, Leningrad (in Russian)
208. Lugin LI (1970) PhD Thesis. Institute of Material Science Problems, Ukrainian Academy of Sciences, Kiev
209. Lopato LM, Lugin LI, Shevchenko AV (1971) Zh Neorg Khim 16: 254
210. Leonov AI, Andreeva AB, Shvaiko-Shvaikovsky VE, Keler EK (1966) Neorg Mater 2: 517
211. Lopato LM, Lugin LI, Gerasimyuk GI (1972) Ukr Khim Zh 38: 143
212. Lopato LM (1976) Ceram Int 1: 18
213. Mayster IM, Lopato LM (1973) Neorg Mater 9: 64
214. Mayster IM, Shevchenko AV, Lopato LM (1982) Neorg Mater 18: 1589
215. Leonov AI, Pirutko MM, Keler EK (1966) Izv Akad Nauk SSSR Ser Khim (5): 90
216. Bazuev GV, Makarova OV, Shveikin GP (1978) Zh Neorg Khim 23: 1451
217. Bazuev GV, Shveikin GP (1977) Zh Neorg Khim 22: 1239
218. Bazuev GV, Shveikin GP (1975) Neorg Mater 11: 2195
219. Zakharov NA, Stefanovich SYu, Kustov EF, Venevtsev YuN (1980) Krist Techn 15: 29
220. Belov BF, Gorokh AV, Demchuk VP (1983) Neorg Mater 19: 256
221. Leonov AI, Keler EK, Andreeva AB (1966) Neorg Mater 2: 1047
222. Leonov AI, Andreeva AB, Keler EK (1966) Neorg Mater 2: 137
223. Savchenko EP, Godina NA, Keler EK (1967) Solid-state reactions between niobium and tantalum pentoxides and rare-earth element oxides. In: Toropov NA (ed) Chemistry of high-temperature materials. Nauka, Leningrad, pp 99–105 (in Russian)
224. Pluschev VE, Amosov VM (1964) Dokl Akad Nauk SSSR 157: 131
225. Lopato LM, Shevchenko OV, Kiryakova IE (1968) Dokl Akad Nauk USSR Ser B 9: 826
226. Krylov EI, Borisov AK, Kazantsev VV (1973) Neorg Mater 9: 269
227. Bazuev GV, Shveikin GP (1985) Complex oxides of elements with completing d- and f-shells. Nauka, Moscow (in Russian)
228. Volchenkova ZS, Palguev SF (1963) Trudy Inst Elektrokhim 4: 67
229. Volchenkova ZS, Palguev SF (1960) Trudy Inst Elektrokhim 1: 127
230. Savenko VG, Sakharov VV, Korovin SS (1975) Trudy Mosk Inst Tonkoy Khim Tekhnol (5): 58
231. Trunov VK, Kovba LM (1963) Vestn Mosk Univ Ser 2 18: 60
232. Spitsyn VI, Pokrovsky AN, Afonsky NS, Trunov VK (1969) Dokl Akad Nauk SSSR 188: 1065
233. Bushuev NN, Trunov VK (1970) Radiokhimiya 12: 411
234. Trunov VK, Bushuev NN (1969) Radiokhimiya 11: 245
235. Spitsyn VI, Falikman VR, Spiridonov FM (1976) Zh Neorg Khim 21: 2593
236. Permyakov PG, Korshunov BG, Krokhin VA (1976) Tsvet Metall (3): 95
237. Vecher AA, Savitsky AA, Shishkov NV, Voropaev AG, Samokhval VV, Zaletova ND (1980) Neorg Mater 16: 1572
238. Lang HY, Ullmann H, Reets T, Teske K, Blayer A, Kant H, Shirrmeyster F, Felts A (1990) Elektrokhimiya 26: 1509
239. Vecher DV (1970) PhD Thesis. Moscow State University, Moscow
240. Samokhval VV (1999) DSc Thesis. Belarus State University, Minsk
241. Murygin IV (1991) Electrode processes in solid electrolytes. Nauka, Moscow (in Russian)
242. Vecher AA, Vecher DV (1968) Zh Fiz Khim 42: 799
243. Vecher DV, Vecher AA (1970) Vesti Akad Nauk BSSR Ser Khim (1): 113
244. Tretyakov JuD, Muan A (1969) J Electrochem Soc 116: 331

245. Vecher AA, Vecher RA, Geiderikh VA, Vasilyeva IA (1965) Zh Fiz Khim 39: 2080
246. Vecher AA, Savitsky AA (1984) Dokl Akad Nauk BSSR 28: 825
247. Vasilyeva IA, Sukhushina IS, Granovskaya ZhV, Balabaeva RF, Mayorova AF (1975) Zh Fiz Khim 49: 2169
248. Samokhval VV, Loiko GI, Vecher AA (1973) Zh Fiz Khim 47: 2275
249. Kuzin BL, Glumov MV (1976) Trudy Inst Elektrokhim 24: 115
250. Shkerin SN (1989) PhD Thesis. Institute of Electrochemistry, Ural Dept. of Academy of Sciences of USSR, Sverdlovsk
251. Arzhannikov VA (1985) PhD Thesis. Institute of Electrochemistry, Ural Dept. of Academy of Sciences of USSR, Sverdlovsk
252. Naumovich EN, Kharton VV, Kovalevsky AV, Samokhval VV (1996) Conjugate transport of oxygen ions and electrons in fluorite-type ceramics $Ce(Gd,M)O_{2-\delta}$ (M = Co, Mn). In: Poulsen FW, Bonanos N, Linderoth S, Mogensen M, Zachau-Christiansen B (eds) Proceedings of the 17th Riso International Symposium on Materials Science. Riso National Laboratory, Roskilde, pp 375–380
253. Perfilyev MV, Palguev SF (1965) Trudy Inst Elektrokhim 6: 107
254. Perfilyev MV, Palguev SF (1965) Trudy Inst Elektrokhim 6: 115
255. Perfilyev MV, Palguev SF (1965) Trudy Inst Elektrokhim 7: 157
256. Perfilyev MV, Palguev SF (1965) Trudy Inst Elektrokhim 7: 163
257. Perfilyev MV, Palguev SF, Karpachev SV (1965) Elektrokhimiya 1: 90
258. Chebotin VN, Glumov MV, Palguev SF, Neuimin AD (1971) Elektrokhimiya 8: 491
259. Somov SI, Perfilyev MV (1990) Polarization characteristics of $CO + CO_2/M + CeO_{2-x}/0.91ZrO_2 + Y_2O_3$ electrode system. In: Perfilyev MV (ed) Electrode reactions in solid electrolytes. Academy of Sciences of USSR, Ural Dept., Sverdlovsk, pp 80–90 (in Russian)
260. Kuzin BL, Demin AK (1988) Electro-reduction of water on Pt-CeO_{2-x} electrode in contact with solid oxide electrolyte. In: Perfilyev MV (ed) Electrode processes in solid electrolyte systems. Academy of Sciences of USSR, Ural Dept., Sverdlovsk, pp 58–66 (in Russian)
261. Kuzin BL, Bronin DI (1993) Elektrokhimiya 29: 279
262. Perfilyev MV (1993) Polarization of platinum-based electrode in the cell with solid oxide electrolyte in the atmospheres $CO + CO_2$ and $H_2 + H_2O$. In: Perfilyev MV (ed) Ionics of solid state. Nauka, Ekaterinburg, pp 76–80 (in Russian)
263. Kuzin BL, Perfilyev MV (1985) On conjugate electro-reduction of H_2O and CO_2 in the cells with solid oxide electrolyte. In: Proceedings of the 2nd Soviet Symposium on Solid Electrolytes and Their Analytical Application. Academy of Sciences of USSR, Ural Dept., Sverdlovsk, pp 155–156 (in Russian)
264. Kharton VV, Naumovich EN, Tikhonovich VN, Bashmakov IA, Boginsky LS, Kovalevsky AV (1999) J Power Sources 77: 242
265. Fadeev GI, Perfilyev MV (1988) Studying equilibrium potentials of gas electrodes of the cells with the ZrO_2-Y_2O_3 electrolyte at reduced temperatures by the thermo-e.m.f. method. In: Perfilyev MV (ed) Electrode processes in solid electrolyte systems. Academy of Sciences of USSR, Ural Dept., Sverdlovsk, pp 85–95 (in Russian)
266. Gorelov GP, Kurumchin EKh (1986) Kinet Katal 27: 1346
267. Gorelov GP, Kurumchin EH (1993) Study of cerium dioxide by the method of isotopic exchange with carbon dioxide. In: Perfilyev MV (ed) Ionics of solid state. Nauka, Ekaterinburg, pp 46–53 (in Russian)
268. Tikhonovich VN, Kharton VV, Naumovich EN, Savitsky AA (1998) Solid State Ionics 106: 197
269. Naumovich EN, Kharton VV, Vecher AA (1998) Ceramic materials for high-temperature electrochemical devices. In: Sviridov VV (ed) Chemical problems of developing new materials and technologies. Belarus State University, Minsk, pp 431–450 (in Russian)
270. Kharton VV, Naumovich EN, Tikhonovich VN, Vecher AA, Samokhval VV (1996) Vestn Belorus Univ Ser 2 (1): 3
271. Tikhonovich VN, Kharton VV, Naumovich EN (1997) Inorg Mater 33: 602
272. Kharton VV, Yaremchenko AA, Naumovich EN (1999) J Solid State Electrochem 3: 303
273. Salzano JF, Isaaks HS, Minushkin B (1971) J Electrochem Soc 118: 416
274. Hardaway JB, Patterson JW, Wilder DR (1971) J Am Ceram Soc 54: 94
275. Shores DA, Rapp RA (1971) J Electrochem Soc 118: 1107
276. Kurumchin EKh (1997) DSc Thesis. Institute of High-Temperature Electrochemistry RAS, Ekaterinburg
277. Kurumchin EKh (1990) Study of the boundary oxygen-electrolyte based on ZrO_2, Bi_2O_3 or CeO_2 by the oxygen isotopic exchange method. In: Perfilyev MV (ed) Electrode reactions in solid electrolytes. Academy of Sciences of USSR, Ural Dept., Sverdlovsk, pp 63–79 (in Russian)
278. Kurumchin EKh, Perfilyev MV (1990) Solid State Ionics 42: 129
279. Sazonov LA, Ratov AN, Ratova TT (1965) Kinet Katal 6: 836
280. Sokolovsky VD, Sazonov LA, Boreskov GK, Moskvina ZV (1968) Kinet Katal 8: 130
281. Sokolovsky VD, Mitrofanova GN, Sazonov LA (1970) Kinet Katal 11: 804
282. Minachev KhM, Antoshin GV (1965) Dokl Akad Nauk SSSR 161: 122
283. Kuzin BL, Perfilyev MV, Gorelov VP, Beresnev SM, Kleschev YuN (1997) Elektrokhimiya 33: 1475
284. Gorelov VP, Arestova NV, Kurumchin EKh, Vdovin GK (1995) Neorg Mater 31: 370
285. Etsell TH, Flengas SN (1970) Chem Rev 70: 339